The Journal of Undergraduate Research in Physics

Volume 16, Number 1
Fall, 1997

Produced by the Physics Department of Guilford College
for
The American Institute of Physics and the Society of Physics Students

THE JOURNAL OF UNDERGRADUATE RESEARCH IN PHYSICS

This journal is devoted to research work done by undergraduate students in physics and its related fields. It is to be a vehicle for the exchange of ideas and information by undergraduate students. Information for students wishing to submit manuscripts for possible inclusion in the Journal follows.

ELIGIBILITY
The author(s) must have performed all work reported in the paper as an undergraduate student(s). The subject matter of the paper is open to any area of pure or applied physics or physics related field.

SPONSORSHIP
Each paper must be sponsored by a full-time faculty member of the department in which the research was done. A letter from the sponsor, certifying that the work was done by the author as an undergraduate and that the sponsor is willing to be acknowledged at the end of the paper, must accompany the manuscript if it is to be considered for publication.

SUBMISSION
Two copies of the manuscript, the letter from the sponsor and a telephone number or E-Mail address where the author can be reached should be sent to:
Dr. Rexford E. Adelberger, Editor
THE JOURNAL OF UNDERGRADUATE RESEARCH IN PHYSICS
Physics Department
Guilford College
Greensboro, NC 27410

FORM
The manuscript should be typed, double spaced, on 8 1/2 x 11 inch sheets. Margins of about 1.5 inches should be left on the top, sides, and bottom of each page. Papers should be limited to fifteen pages of text in addition to an abstract (not to exceed 250 words) and appropriate drawings, pictures, and tables. Manuscripts may be submitted on a disk that can be read by a MacIntosh™. The files must be compatible with MacWrite™, MicroSoft Word™ , PageMaker™ or WordPerfect™.

ILLUSTRATIONS
Line drawings should be made with black ink on plain white paper. The line thickness should be sufficient to be reduced to column format. Each figure or table must be on a separate sheet. Photographs must have a high gloss finish. If the submission is on a disk, the illustrations should be in PICT, TIFF or EPS format.

CAPTIONS
A descriptive caption should be provided for each illustration or table, but it should not be part of the figure. The captions should be listed together at the end of the manuscript

EQUATIONS
Equations should appear on separate lines, and may be written in black ink. All equations should be numbered. We use EXPRESSIONIST™ to format equations in the Journal.

FOOTNOTES
Footnotes should be typed, double spaced and grouped together in sequence at the end of the manuscript.

PREPARING A MANUSCRIPT
A more detailed set of instructions for authors wishing to prepare manuscripts for publication in the Journal of Undergraduate Research in Physics can be found in the back of each issue.

SUBSCRIPTION INFORMATION

The Journal is published twice each academic year, issue # 1 appearing in the fall and issue # 2 in the spring of the next calendar year. There are two issues per volume.

TYPE OF SUBSCRIBER	PRICE PER VOLUME
Individual	$US 5.00
Institution	$US 10.00

Foreign subscribers add $US 2.00 for surface postage, $US 10.00 for air freight.

Back issues may be purchased by sending $US 15.00 per volume to the editorial office.

To receive a subscription, send your name, address, and check made out to **The Journal of Undergraduate Research in Physics (JURP)** to the editorial office:

JURP
Physics Department
Guilford College
Greensboro, NC 27410

The Journal of Undergraduate Research in Physics is sent to each member of the Society of Physics Students as part of their annual dues.

VOLUME 16

ACADEMIC YEAR 1997-1998

The Journal of Undergraduate Research in Physics

ISSN 0731 - 3764

Produced by the Physics Department
of Guilford College
for
The American Institute of Physics
and
The Society of Physics Students

$Si_{16}X_4$ (X=N, P, As): Deactivated Si Clusters?

Max Dkysterhouse and Kevin Smith
Department of Physics
Central Michigan University
Mt. Pleasant, MI 48859
received October 4, 1996

ABSTRACT

Recent local density approximation (LDA) calculations have identified $Zr@Si_{20}$ as a very strongly bound endohedral system [1]. The bonding in this system can be understood on the basis of the electronic structure of the Si_{20} cluster, which has a partially filled highest occupied molecular orbital (HOMO), reducing the bonding of these clusters to endohedral atoms, leaving them deactivated. We present results of LDA calculations on these clusters. We compare the structural and electronic properties of the $Si_{16}X4$ clusters with those of Si_{20}. We also compare the binding energies of these clusters to the endohedral Zr atom and the exohedral H. We find the binding energy reduced in the substituted clusters. The calculations predict $Si_{16}N_4$ to be particularly stable, suggesting that it could be readily produced experimentally.

1. Jackson and Nellermoe, Chem. Phys. Lett., 254, (1996), p. 249.

INTRODUCTION

In the development of new and novel materials, a new technique of fabrication may be emerging out of the field of cluster research. Recently, it has been suggested that new "superatoms", small clusters of atoms that behave and react with other clusters or atoms as a single unit, might be used to form new unique materials. The A_nC_{60} compounds made from the C_{60} buckyball are examples of cluster based materials.

The area of cluster research is relatively new. Techniques for creating and characterizing clusters experimentally are still being developed. However, it is possible to study cluster properties theoretically using accurate, first principles methods. Specifically, we want to know about the stability and chemical reactivity of these clusters. Such characteristics need to be understood to make cluster-based materials fabrication a reality.

Some attention has recently been given to the C_{28} and Si_{20} clusters, which are similar in several ways [1-7]. The cage-like isomers (see Figure 1a) of these clusters are not stable by themselves. However, two approaches have been suggested to stabilize these clusters. One way is to introduce an additional, foreign, so-called endohedral atom (see Figure 2a) into the center of the clusters [5]. This endohedral atom bonds strongly with the cage of the cluster, stabilizing the structure. Another approach is to replace some cage atoms with foreign atoms (see Figure 2b and 2c) to give a more stable electronic structure [8]. For example, both C_{28} and Si_{20}, the cluster needs four electrons to fill the cluster electronic shell. Substituting four Group V atoms (e.g., N, As, P, etc.) into the cage

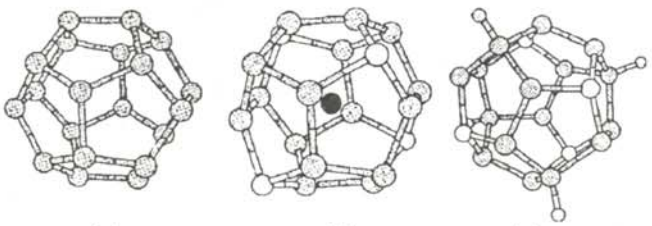

(a) (b) (c)

Figure 1

Schematic diagrams of (a) cage structure of Si_{20} (b) cage structure with 4 substituted atoms and with endohedral atom at the center, $Zr@Si_{16}P_4$ (c) structure showing external bound hydrogen atoms, $Si_{16}P_4H_4$.

Max is a senior at Central Michigan University, studying German and chemistry. Last year he concentrated on his German while studying in München, Germany for a year. He is completing his undergraduate studies and will be applying to graduate schools in biochemistry.

Kevin graduated with a B.Sc. in physics and electronics engineering technology from Central Michigan University in 1966. He is currently a graduate student at North Carolina State University in the Department of Electrical Engineering. In his spare time, he enjoys working on his Linux PC and developing web pages.

brings four extra electrons to the cluster, leaving the cluster with a closed shell electronic structure analogous to a noble gas atom.

The study of $C_{24}X_4$ (X=N, P, As) has shown that the introduction of the Group V atoms produces a gap between the highest occupied molecular orbital (HOMO) and the Lowest unoccupied molecular orbital (LUMO), rendering the cluster chemically more stable [8]. These results illustrate an important aspect of using clusters as a basis for advanced materials: it is possible to tailor the properties of the "superatoms" for a particular application. In this paper, we study in detail the analogous $Si_{16}X_4$(X=N, P, As) clusters. We investigate the stability of the clusters and the bonding to external hydrogen atoms and the endohedral Zr atom as shown in Figures 1b and 1c.

COMPUTATIONAL METHODS

To explore the properties of silicon and doped silicon clusters, we used a quantum mechanical approach since our interest is in bonding which is an inherently quantum mechanical process. Our calculations are based on the Local Density Approximation (LDA), a first-principles quantum mechanical method [9]. The LDA models the electron-electron interaction to make practical calculations for many electron systems possible. In the LDA, a Schrödinger-like equation is solved self consistently to yield orbitals and energy levels for all the electrons in the cluster. The orbitals are then used to compute the total energy of the system and the forces on the atoms. Experience has shown that the LDA works well to describe electronic and structural properties of molecules and solids, including systems of all types and involving atoms from across the periodic table. For example, bond lengths obtained with LDA calculations are within 1% to 2% of experimental values [10]. The specific approach we use employs Gaussian basis sets to represent the electron orbitals [11,12]. The calculations were executed on UNIX workstations, each taking a couple of hours of CPT time per energy calculation.

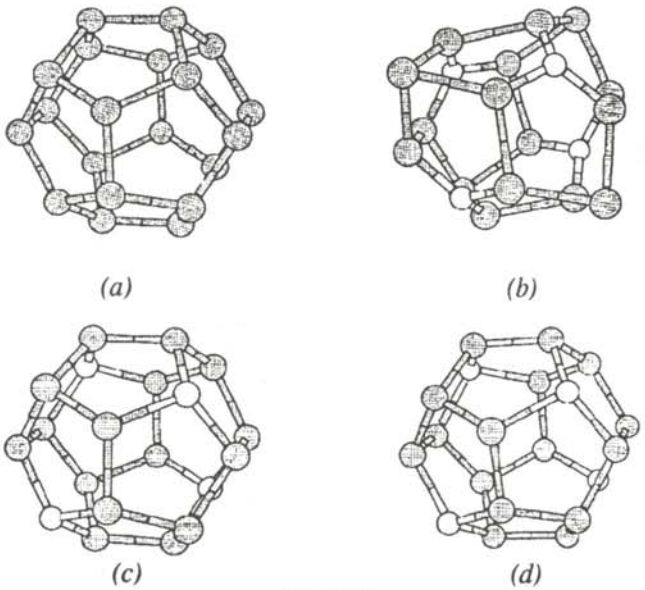

Figure 2
The structures of: (a) Si_{20}, (b) $Si_{16}N_4$, (c) $Si_{16}P_4$, (d) $Si_{16}As_4$

The first step in studying the properties of a cluster is to determine the optimal arrangement of the atoms. This corresponds to the structure with the lowest energy. To find the minimum energy, we use a conjugate-gradient algorithm. This procedure systematically shifts the positions of each atom according to the forces induced by the neighboring atoms. The atoms are moved until the forces on each atom vanish. For Si_{20}, symmetry constraints were imposed on the cluster structure to maintain the high symmetry of the cage. The resulting relaxed configuration was used as a starting point for the other silicon clusters doped with one of the three group V elements. In these clusters four symmetric silicon atoms were replaced with nitrogen, phosphorus or arsenic. The doped clusters were then allowed to relax with the symmetry constraints reduced to accommodate the atomic substitutions.

RESULTS

Cluster Structures

The four clusters studied are shown in Figure 2. The Si_{20} cluster, Figure 2a, subjected to the symmetry constraint, had an average bond length of 2.27 Å. The bulk Si-Si bond length is 2.348 Å. This shorter bond length suggests a partial multiple bond character. The cage structure is not stable; it distorts if the symmetry constraint is removed. This is due to a partially filled HOMO level.

We chose three different group V atoms to replace four of the atoms in the Si cluster as seen in Figure 2. The atoms were substituted symmetrically around the cluster. Each of these atoms contributes one valence electron to the structure, thus filling the outermost electron shell and opening a HOMO-LUMO gap.

The $Si_{16}N_4$ cluster, Figure 2b, shows considerable distortion from the Si_{20} geometry. This is due to the large size difference between nitrogen and silicon. The atomic radius of nitrogen is 0.70Å and the radius of silicon is 1.17Å. The optimal Si-N bond length is therefore much shorter than the Si-Si bond. The bond lengths in the cluster are 1.78Å for Si-N and 2.36Å for Si-Si. With these shorter bonds, the cluster distorts significantly in relaxing to the final minimum energy configuration.

The phosphorus doped cluster, shown in Figure 2c, showed very little distortion from the Si_{20} shape. The average Si-Si bond length was 2.31Å and the average Si-P bond length was 2.26Å. The similarity in the bond lengths is due to the similarity in the atomic radii of silicon and phosphorus (1.10Å). The same is true for the arsenic doped cluster shown in Figure 2d. The arsenic atom has a radius of 1.21Å. The arsenic doped cluster has an average Si-Si length of 2.31Å and an average Si-As bond length of 2.37Å.

HOMO-LUMO gaps

In Figure 3, we show the energy level diagrams for the clusters calculated by the LDA. Only the levels associated with the valence electrons are shown. The overall spherical shape of the Si_{20} cluster is reflected in the angular character of the molecular orbital states of the cluster [7]. This angular character is approximately that of atomic orbitals (which are eigenstates of a spherically symmetric potential), hence the labels '*s*', '*p*', '*d*', etc., for the cluster states in Figure 3. The degeneracies of the levels in the electronic structure are suggestive of the approximately spherical nature of the potential. The degeneracies are arranged in the order: 1-fold, 3-fold, 5-fold, etc., as they are for s, p, d-type orbitals, etc. The specific degeneracies are not shown in Figure 3, but the levels are labeled according to their angular character. Note that the symmetry of the cluster potential is not perfectly spherical, so that the degeneracy of the levels beyond '*d*' is broken in the cluster. Because of the presence of the Group V atoms, the other clusters have lower symmetry than Si_{20}. This results in fewer degeneracies of the electronic levels as can be seen in Figure 3.

One rough measure of the chemical reactivity of the clusters are the HOMO-LUMO gaps given in Table 1. Generally a larger gap implies than an electron requires more energy to break a bond to form a new bond with a reactant, so the larger the gap, the less reactive the molecule. There are four vacancies or holes in the Si_{20} HOMO level, represented in Figure 3 by the four circles at the highest occupied level. The bare Si_{20} cluster thus has an open electronic shell and should be quite reactive.

When nitrogen is substituted into the Si_{20} cluster, a HOMO-LUMO gap of 0.16 eV opens up. This is in agreement with our expectations bases on counting valence electrons. The electronic structure of $Si_{16}N_4$, shown in Figure 3, stands out from the others in that it is much more spread out in energy. There are fewer degeneracies among the levels. The decrease in degeneracies is due to the reduced symmetry of the $Si_{16}N_4$ cluster, due both to the presence of the nitrogen and because of the significant distortion from the spherical cage. The width of the spectrum can be attributed to nitrogen's strong electronegativity. This can be viewed in terms of the energy levels of the N and Si atoms. For example, the nitrogen 2S valence electron in the free atom lies at -0.731 a.u. compared to -0.416 a.u. for the silicon 3S state. In the cluster, the molecular orbital state is around -0.78 a.u. correspond to combinations of the nitrogen 2S orbitals. (Atomic Units of energy, a.u., are convenient for electronic structure calculations; 1 a.u. = 27.21 eV.)

HOMO-LUMO energy gap	
Si_{20}	0 eV
$Si_{16}N_4$	0.160 eV
$Si_{16}P_4$	0.376 eV
$Si_{16}As_4$	0.361 eV

Table 1

The energy separation between the highest occupied molecular orbital (HOMO) and the lowest unoccupied molecular orbital (LUMO) for each cluster.

The HOMO-LUMO gaps of $Si_{16}P_4$ and $Si_{16}As_4$ are shown in Table 1. Because the atomic structure of these clusters is very similar to that of Si_{20}, some of the degeneracy seen in the energy level diagram of Si_{20} is regained.

Binding Energies

Recently it has been shown that $Zr@Si_{20}$, (a Si_{20} cluster with an endohedral Zr atom at the center), has a very large binding energy between the Zr and the cage [7]. Apparently, the Zr atom bonds with the dangling bonds of the cage. We found that Zr introduced into the $Si_{16}P_4$ cluster (Table 2 and Figure 1b) was less energetically favorable. The binding energy of the Zr was reduced by 2.09 eV. This decrease can be attributed to the increased chemical stability of the $Si_{16}P_4$ cluster due to the opening of the HOMO-LUMO gap.

The hydrogenation of Si_{20} gives another reference point for investigating the chemical reactivity of the $Si_{16}X_4$ clusters. As shown in Table 2, in $Si_{20}H4$, each Si-H bond has a strength of 3.5 eV. This binding is reduced to 3.0 eV and 2.8 eV in the doped clusters $Si_{16}P_4H_4$ and $Si_{16}N_4H_4$.

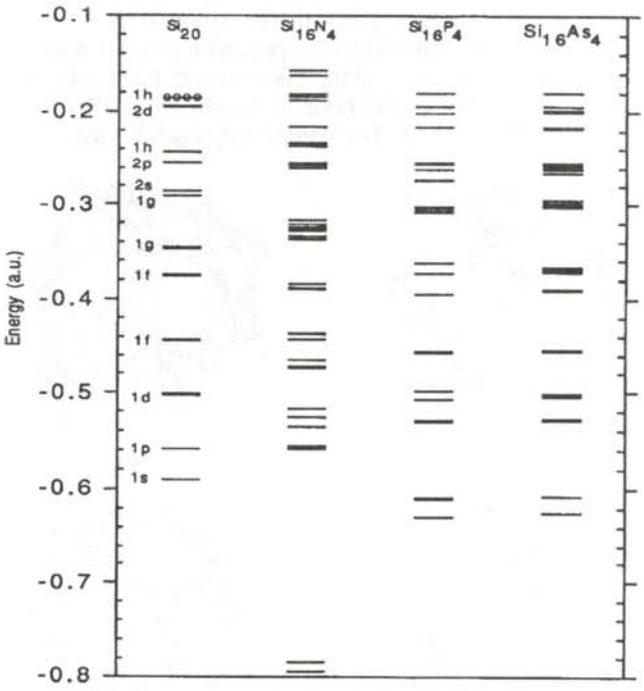

Figure 3

The electronic structure of Si_{20} and the $Si_{16}X_4$ clusters. There are four "holes" at the HOMO level in Si_{20}. The dashed lines represent the LUMO levels. Energy is in atomic units (1 a.u. = 27.21 eV)

Again, the closed shell nature of the doped clusters is seen to reduce the binding to reactants.

Cluster Energetics

It is interesting to consider the question of whether the doped clusters could be formed in an experiment. While the detailed mechanism of Si cluster formation is not known, we can gain some insight by considering the stability of the clusters with respect to other molecular species. We looked at the energy of formation of the clusters, ΔQ, using:

$$\Delta Q = E(Si_{16}X_4) - \frac{16}{10} E(Si_{10}) - \frac{4}{n} E(X_n) \qquad (1)$$

where X= N, P, or As. Equation 1 represents the energy gained in the dissociation to Si_{10} and X_n clusters. Si_{10} is considered because it has the largest binding energy per atom of any silicon cluster in the small to intermediate range including the most stable Si_{20} structure known [13]. X_2 and X_4 are considered since N_2 is the most stable arrangement of N atoms, and P_4 and As_4 are stable arrangements of those atoms [8]. The extreme situation of dissociation to free atoms occurs when $n = 1$.

If ΔQ is negative, no energy is gained via dissociation and the $Si_{16}X_4$ is stable. Figure 4 is a plot of ΔQ versus the inverse of n for the various clusters studied. The plot for nitrogen shows $\Delta Q<0$ for all n. This implies that $Si_{16}N_4$ is energetically favorable compared to all reasonable dissociation pathways. This suggests that it could be possible to produce this cluster experimentally. Once formed, it would not be likely to dissociate. However, this analysis only considers relative energetics and does not take into account kinetic factors which may hinder the formation of $Si_{16}N_4$ under experimental conditions.

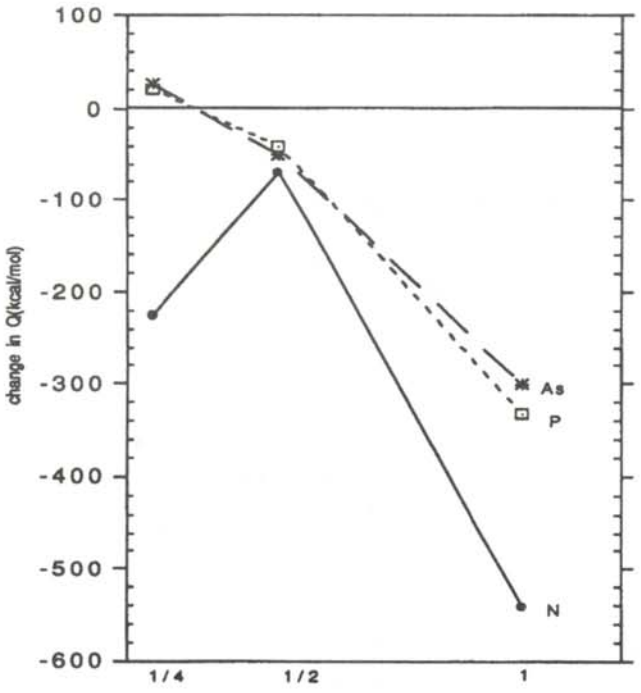

Figure 4

A plot of the change in Q from Equation 1 versus the inverse of n in X_n.

Cluster	E_B
$Zr@Si_{20}$	15.20 eV
$Zr@Si_{16}P_4$	13.11 eV
$Si_{20}H_4$	3.5 eV/H
$Si_{16}P_4H_4$	3.0 eV/H
$Si_{16}N_4H_4$	2.8 eV/H

Table 2

Binding energies of clusters. The binding energy of the endohedral Zr is computed with respect of the isolated endohedral atom and the cluster. The binding energy of the exohedral hydrogen is calculated with respect to the isolated hydrogen atom the cluster.

The curves for $Si_{16}P_4$ and $Si_{16}As_4$ show a positive ΔQ when $n = 4$ so these clusters are unstable against dissociation to Si_{10}'s and X_4's. This suggests that these clusters would be difficult to produce in experiments since they would favor spontaneous dissociation to other structures.

There are two potential problems with these predictions. First, a well known problem with the LDA is that it tends to overbind molecules with respect to free atoms. This introduces some uncertainty into the binding energy results shown in Figure 4. However, since the computed results compare the LDA energies for various molecules, there will be some cancellation of overbinding errors. Therefore, we believe the results in Figure 4 are at least qualitatively correct. It would be interesting to recompute the relevant binding energies using the new generalized gradient approximations which have been found to improve on the LDA binding energies. [14].

A second issue affecting our prediction involves the kinetics of cluster formation. It is possible that formation of cage like clusters as shown in Figure 1 first require forming smaller, quasi-planar clusters that then combine to form a closed cage. Such precursors are thought to be important in fullerene formation. Such planar structures are unlikely in bare silicon clusters since these tend to be close-packed and three dimensional. However, with nitrogen atoms present, small Si_nN clusters may favor more open geometries and thus provide the needed precursors for cage production. For this reason, it would be interesting to consider the structures of small Si_nN clusters.

ACKNOWLEDGMENT

The authors wish to acknowledge the support of the NSF through grant RUI-DMR940985

REFERENCES

* Current address of author: 11229 Snows Lake Road, Greenville, MI 48838.

† Current address of author: 2300 Avent Ferry Road, Apt. H3, Raleigh, NC 27606.

1. T. Guo, e.. al., Science, 257, (1992), p. 1661
2. B.I. Dunlap, O.D. Haberlen and N. Rosch, J. Phys. Chem., 96, (1992), p. 9095; O.D. Haberlen, N. Rosch and B.I. Dunlap, Chem. Phys. Lett., 200, (1992), p. 200.
3. M.R. Pederson and N. Laouini, Phys. Rev. B, 48, (1993), p. 2733.
4. K.A. Jackson, E. Kaxiras and M.R. Pederson, Phys. Rev. B, 48,17, (1993), p. 556.
5. K. Jackson, E. Kaxiras and M.R. Pederson, J. Phys. Chem., 98, (1994), p. 7805.
6. J. Grossman and L. Mitas, Phys. Rev. Lett., 74, (1995), p. 1323.
7. K.A. Jackson and B. Nellermore, Chem. Phys. Lett., 254, (1996), p. 254.
8. E. Kaxiras, K.A. Jackson and M.R. Pederson, Chem. Phys. Lett., 225, (1994), p. 448.
9. P. Hohenberg and W. Kohn, Phys. Rev. B, 136,(1964), p. 864; w. Kohn and L.J. Sham, Phys. Rev. A., 140, (1965), p. 1133.
10. R.O. Jones and O. Gunnarson, Rev. Mod. Phys., 61, (1989), p. 689.
11. M.R. Pederson and K.A. Jackson, Phys. Rev. B., 41, (1990), p. 7453.
12. K.A. Jackson and M.R. Pederson, Phys. Rev. B, 42, (1990), p. 3276.
13. M.R. Pederson, K.A. Jackson, D.V. Porezag, Z. Hajnal and Th. Frauenheim, Phys. Rev. B, 54, (1996), p. 2863.
14. J.P. Perdew, J.A. Chevary, S.H. Vosko, K.A. Jackson, M.R. Pederson, D.J. Singh and C. Fiolhais, Phys. Rev. B., 46, (1992), p. 6671.

FACULTY SPONSOR

Dr. Koblar Jackson
Physics Department
Central Michigan University
Mt. Pleasant, MI 48859

EVALUATION OF THICK TARGET YIELDS OF DEUTERON INDUCED GAMMA RAY EMISSION FROM Li, B, N, F, Na and Mg

Zoltán Elekes
Institute of Nuclear Research of the Hungarian Academy of Science
Department of Nuclear Physics
Debrecen, Hungary, 4028
received May 1, 1997

ABSTRACT

Ion beams have been used for elemental analysis of different samples for decades. In the determination process of sample composition, thick target gamma ray yields of charged particle induced gamma ray emission play a very important role. For light elements, the deuteron induced gamma ray emission method is the most favorable. For six elements (Li, B, N, F, Na and Mg) the investigation of gamma peaks were carried out. The gamma ray yields were evaluated and yield curves were determined in the bombarding deuteron energy range of 0.7 - 3 MeV.

INTRODUCTION

Ion beams have been used for elemental analysis of different samples for decades. [1,2] The steps used to determine elemental composition are:

- selection of the most favorable technique based on different ion-matter interactions from the point of view of the given sample: irradiation conditions, detection techniques, consideration of background and interfering interactions.
- measurement of the intensity of radiation with respect to some measured quantity of the bombarding ion (in most cases, the charge collected on the sample).
- conversion of the net yield of radiation into a concentration of the unknown element by means of known reaction yields or from the measured yield of a sample of known composition.

It is basically important to know the reaction yield, i.e. the quantity of particles produced in the sample by a unit bombarding ion (if the sample consists only of the unknown element, and to evaluate the concentrations of the unknown element).

For the determination of the concentration of light elements, the Proton Induced Gamma-ray Emission (PIGE) method is widely used because of the following practical reasons:

- a lot of samples can be measured in a short time
- good resolution can be achieved with Ge(Li) or HpGe detectors
- it is not necessary to place the detector in a vacuum
- simultaneous measurements can be performed with Proton Induced X-ray Emissions (PIXE), a complementary method for heavier elements.

The greatest disadvantage of this method is that the spectra are very complex because of the photo-peaks, continuous background (due to multiple Compton scattering) and escape peaks. In the case of some light elements (C, N, O, P, S), using commonly available accelerators with a few MeV bombarding energy, the yields are very small. Thus, these elements can not be detected if the sample contains a small amount of unknown nuclei. The use of deuterons instead of protons as bombarding particles can solve the problem. Thus, tests were done to determine reaction yields using deuterons as bombarding particles. In this paper, the usefulness of Deuteron Induced Gamma-ray Emission (DIGE) method for analytical applications was examined, and the usable reactions and gamma-peaks determined.

Yield evaluations and analytical applications of the DIGE method have been known since the early works of Sparks,

This work was carried out when Zoltán was an undergraduate physics student at Kossuth Lajos University (Debrecen, Hungary). At present, he works for the Institute of Nuclear Research of the Hungarian Academy of Sciences at the Department of Electrostatic Accelerators. His current research interests are in the area of the application of ion beams in archaeometry. He determines the elemental composition of artifacts by means of ion beam analysis, mainly with Particle Induced X-ray Emission and Particle Induced Gamma-ray emission methods.

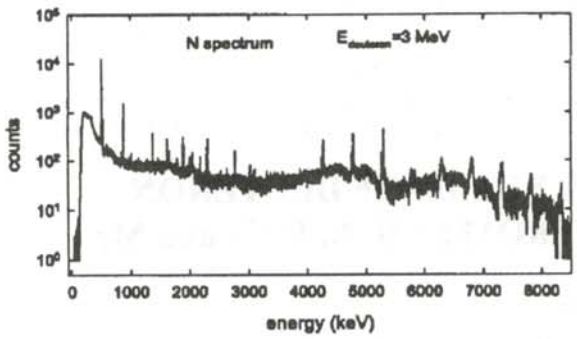

Figure 1
Gamma-ray spectrum of a TaN sample.

et.al.[3], but the real applications of DIGE can be found only in a few articles. [4,5,6,7,8]

The investigations and the thick-target gamma-ray yield evaluations presented here relied on experiments performed at the Research Laboratory of the French Museums (Louvre, Paris) and were carried out for 6 light elements in the bombarding energy range of 0.7 to 3.4 MeV. [9]

Principles of Charged Particle Induced Gamma Ray Emission Measurements

When a sample is bombarded with an ion beam, the incident particles produce nuclear reactions during the interaction with the target nuclei. These reactions can take place either through compound nucleus reactions or via direct reactions in the case of complex (A≥2) bombarding ions. The final nucleus is most often produced in an excited state. This state decays into the ground state by emitting gamma-rays. The energy of the detectable radiation is equal to the energy difference between the energy levels in the target nucleus.

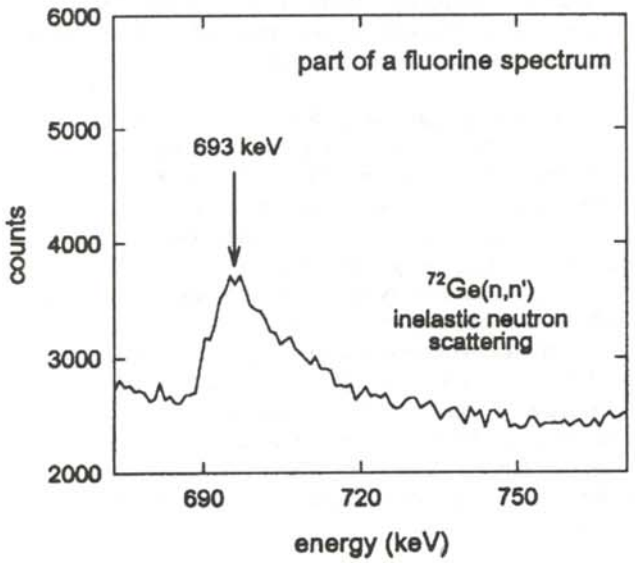

Figure 2
Gamma-ray spectrum produced by ^{72}Ge from $^{72}Ge(n,n')^{72}Ge$ inelastic scattering.

Analog voltage signals are produced in the detector by the photons originating from the transition. These are fed through a linear amplifier and converted into digital signals with an Analog to Digital Converter (ADC). These signals are then displayed on a monitor. An example of a gamma-ray spectrum from a TaN sample is shown in Figure 1. The gamma ray energies are characteristic of the given target nuclei, thus the elemental and isotopic composition of a sample can be determined.

In the case of deuteron capture, the binding energy of the deuteron causes the compound nucleus to be produced in a highly excited state. Therefore, the excitation energy of the compound nucleus greatly exceeds the necessary average energy to separate the final nucleus and an alpha-particle. Thus, in the case of all (d,p), (d,n) and (d,α) reactions, the yield is large.

The stripping reaction, (d,p), takes place in a way such that the proton does not enter the nucleus, so the neutron has only to overcome a small potential barrier to get into the nucleus. Thus it can happen via a tunneling effect. From this, it follows that the (d,p) reaction has an especially large gamma-ray yield.

Problems Associated with the Analysis

The first task is to identify all the gamma-ray peaks and to select suitable ones from the point of view of analytical applications. A number of potential problems arise:

- If the intensity of the bombarding beam is low (for the sake of nondestructive investigation), gamma-ray peaks from the laboratory background radiation can appear in the spectrum.

- It can happen that the gamma-ray peak due to more than one reaction or a peak produced by a different reaction is so close to the peak of interest only one broad peak will appear in the spectrum. This means that the effects of different reactions cannot be separated from each other. For example, if the sample contains fluorine, oxygen and magnesium, the following reactions can happen:

$^{16}O(d,p\gamma_{1\text{-}0})^{17}O$ -> 870.8 keV
$^{16}F(d,\alpha\gamma_{1\text{-}0})^{17}O$ -> 870.8 keV
$^{24}Mg(d,n\gamma_{5\text{-}3})^{25}Al$ -> 872.5 keV

(The notation $\gamma_{1\text{-}0}$ represents the gamma-ray produced by the transition of the final nucleus between its first and ground states. The notation is similar to this.) These gamma peaks are difficult to resolve.

- Neutrons produced during the experiment destroy the detector. They also scatter in the detector in an inelastic way. [10] The backscattered nuclei are in an excited state which decays into the ground state giving an additional signal in the detector [11]. In Figure 2, part of a fluorine

spectrum can be seen. It shows a gamma-ray peak originating from a $^{72}Ge(n,n')^{72}Ge$ reaction.

- The single and double escape peaks can also appear in the spectrum A triplet (full energy peak, single escape peak and double escape peak) can be seen in Figure 3.

- If the lifetime, τ, of the produced excited state is short enough, the final nucleus is moving when the gamma-ray is emitted. In this case, the gamma-ray peak will be broadened due to the kinematic Doppler effect. This effect is shown in Figure 4. The 390 keV peak in Figure 4a is caused by the decay of the second excited state of ^{25}Mg (τ=11ps) found in a magnesium spectrum. There is no broadening in this peak. Contrast this to the Doppler broadened peak at 1885 keV shown in Figure 4b, produced by the decay of ^{15}N (τ=20Fs) from its 4th excited state. The energy calibration and the chosen energy interval (1200 keV) is the same in both of the figures.

In light of these effects and problems, the gamma peaks to be used were chosen for all the six elements (Li, B, N, F, Na and Mg) and the yield calculations started.

The Analysis[12]

After the peaks were selected, the net area under each peak, $S_m(E_\gamma)$, was determined with a gamma spectrum evaluation program. The gamma yield, Y, was determined by:

$$Y = \frac{S_m(E_\gamma)\ \ K_{mx}(E_{deuteron})}{Q\ \Omega\ \eta_{absolute}(E_\gamma)}\ , \qquad (1)$$

where $K_{mx}(E_{deuteron})$ is a correction factor used when

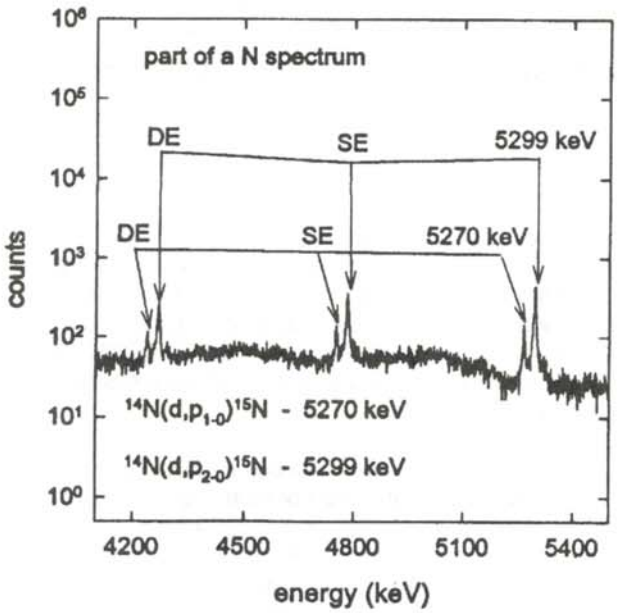

Figure 3

Two gamma-ray peak from the two nitrogen reactions with their escape peaks. SE = Single Escape, DE = Double Escape.

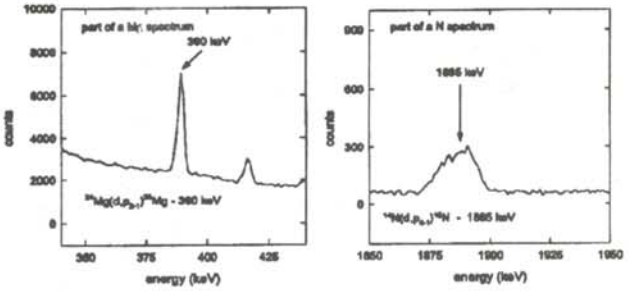

(a) (b)

Figure 4

Comparison between a peak having (a) no Doppler broadening and (b) a peak that is Doppler broadened

samples contain nuclei that are different from the one to be investigated, Q is the collected charge on the sample, Ω is the solid angle of the detector and $\eta_{absolute}(E_\gamma)$ is the absolute efficiency of the detector. Y is measured in units of number of gammas/(micro-Coulomb steradian). The error, derived from uncertainties in the various quantities in Equation 1 is approximately 20%.

Results

Table 1 shows the reactions, the Q values and the gamma energies of the reactions we picked to identify the various light elements. The resulting thick target gamma ray yield curves for the elements are shown in Figure 5. The smooth line behavior of the data points makes calculation

Element	Reaction	Q value MeV	γ energy keV
Li	$^{6}Li(d,p\ \gamma_{1\text{-}0})^{7}Li$	5.026	478
	$^{6}Li(d,n\ \gamma_{1\text{-}0})^{7}Be$	3.381	429
B	$^{11}B(d,p\ \gamma_{1\text{-}0})^{12}B$	1.145	953
	$^{11}B(d,p\ \gamma_{2\text{-}0})^{12}B$	1.145	1674
N	$^{14}N(d,p\ \gamma_{4\text{-}1})^{15}N$	8.609	1885
	$^{14}N(d,p\ \gamma_{6\text{-}1})^{15}N$	8.609	2297
	$^{14}N(d,p\ \gamma_{1\text{-}0})^{15}N$	8.609	5270
	$^{14}N(d,p\ \gamma_{2\text{-}0})^{15}N$	8.609	5299
F	$^{19}F(d,p\ \gamma_{2\text{-}1})^{20}F$	4.377	167
	$^{19}F(d,p\ \gamma_{2\text{-}0})^{20}F$	4.377	823
	$^{19}F(d,p\ \gamma_{3\text{-}0})^{20}F$	4.377	984
	$^{19}F(d,p\ \gamma_{5\text{-}0})^{20}F$	4.377	1309
Na	$^{23}Na(d,\alpha\ \gamma_{1\text{-}0})^{21}Ne$	6.914	350
	$^{23}Na(d,p\ \gamma_{1\text{-}0})^{24}Na$	4.735	472
Mg	$^{24}Mg(d,p\ \gamma_{2\text{-}1})^{25}Mg$	5.107	390
	$^{24}Mg(d,p\ \gamma_{1\text{-}0})^{25}Mg$	5.107	585
	$^{24}Mg(d,n\ \gamma_{2\text{-}1})^{25}Al$	0.047	452

Table 1

The selected gamma-ray peaks and the reactions.

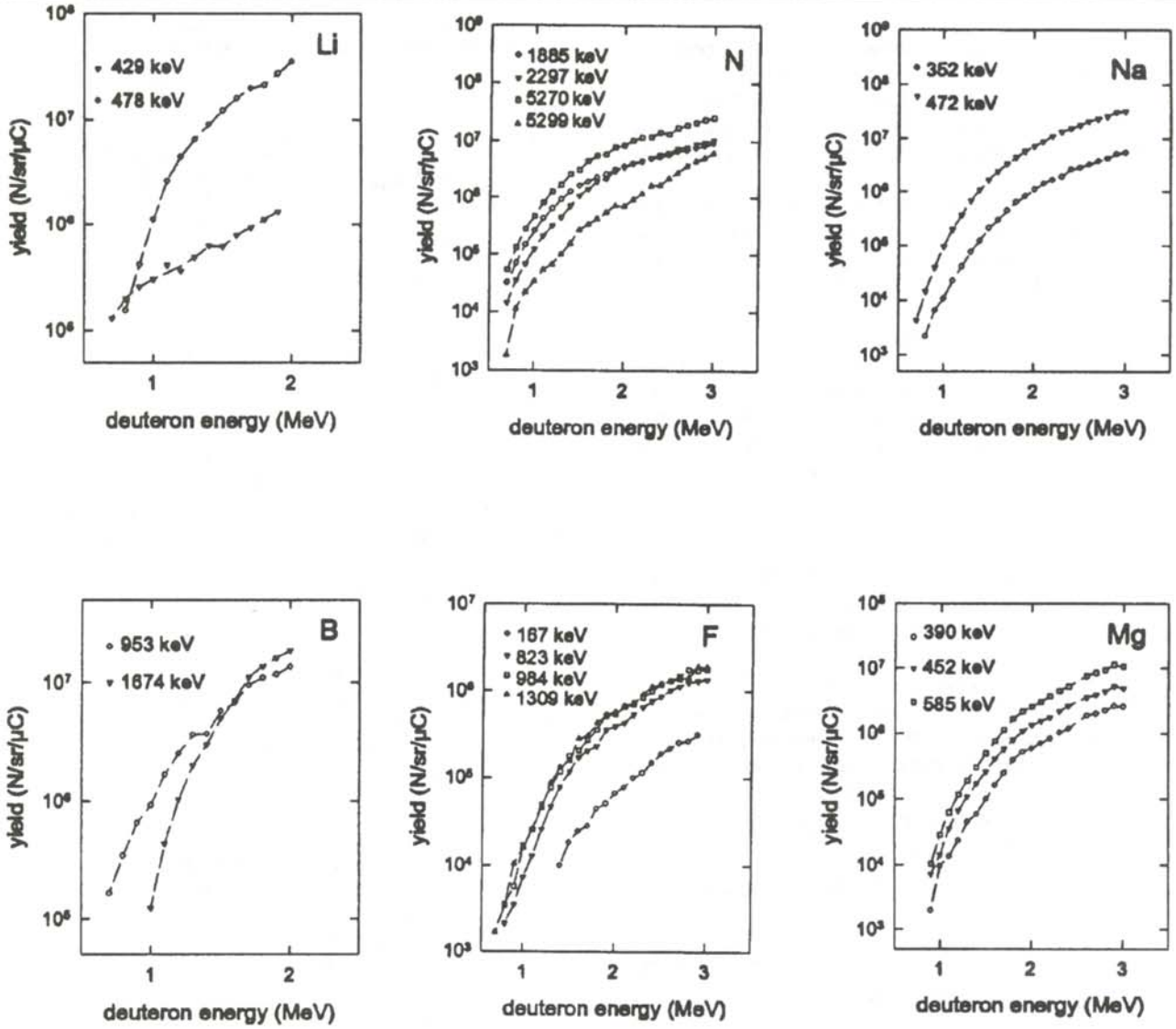

Figure 5
Thick target gamma-ray yield curves for the 6 elements chosen for this experiment.

of yield values between measured values easy.

Table 2 shows our results at E_d = 1.8MeV, (a convenient bombarding energy in many aspects) and compares them with results from PIGE done at a much higher incident energy (E_p = 3.8 MeV). We can conclude that the same gamma yields can be reached with much smaller bombarding energy in the case of DIGE rather than PIGE. Thus, these elements can be detected using DIGE where PIGE identification can be done with a large error due to the poor statistics. In the case of nitrogen, the DIGE method can become especially important.

In the case of fluorine, however, the DIGE yields are smaller than the PIGE yields. If the bombarding deuteron energy increases, the same yield can be reached, but the detection limit will not be better because with DIGE, the peaks are sitting on the Compton edges. However, in the case of PIGE, there is a gamma-ray peak of high energy (6129 keV) the detection limit of which will fall with increasing bombarding proton energy because it is not disturbed by the Compton edges of other peaks. Therefore, for the detection of fluorine, the PIGE method is suggested.

Because of the high deuteron induced gamma ray yields, the DIGE method can provide a potential application in scanning proton microprobes.

ACKNOWLEDGMENTS

The author would like to express his thanks to Dr. Árpád Zoltán Kiss for his encouragement and constructive guidance. This work was supported by the National Research Foundation OTKA (A080)

	DIGE E_d=1.8 MeV		PIGE E_p=3.8 MeV	
Element	γ energy keV	Yield Nγ/μC/str	γ energy keV	Yield Nγ/μC/str
Li	429	1.1(7)	429	9.2(6)
	478	2.1(7)	478	5.6(7)
B	953	1.1(7)	718	1.3(6)
	1674	1.4(7)	2125	4.8(6)
N	1885	2.6(6)	2313	5.5(4)
	2297	2.2(6)	4439	6(4)
	5270	5.5(5)		
	5299	5.8(6)		
F	167	4.4(4)	197	2(7)
	823	2.3(5)	1236	3(6)
	984	3.6(5)	1349	1.3(6)
	1309	4.2(5)	1357	1.4(7)
			6129	9.5(6)
Na	350	6.4(5)	440	9.6(6)
	472	4.5(6)	1635	9.9(6)
Mg	390	3.9(5)	390	6.2(4)
	472	8(5)		
	585	0.7(6)	585	2.2(5)

Table 2
A comparison between PIGE and DIGE gamma-ray yields. The interpretation of the yield values is: X(Y) -> Xx10^Y. For example, 1.1(7) = 1.1x10^7.

REFERENCES

* Current address of the author: Zoltán Elekes, Institute of Nuclear Research of the Hungarian Academy of Sciences, Department of Electrostatic Accelerators, 18/c Bem tér, Debrecen, Hungary, 4028, Elekes@atomki.hu.

1. J.R. Bird and J.S. Williams, Ion Beams for Material Analysis, Academic Press, NY (1989).
2. J.R. Tesmer and M. Nastasi, Handbook of Modern Ion Beam Analysis, Materials Research Society, Pittsburgh, PA, (1995).
3. R.J. Sparks, G.J. McCallum, New Zealand J. Sci., 12 (1969), p. 470.
4. R.J. Sparks, New Zealand Inst. of Nucl. Sci. Rep., INS-R-229, (1977).
5. F. Bodart, G. Deconninck and J. Mengeot, Int. Smyp. on Nuclear Activation Techniques in the Life Sciences, Vienna, 1976, IAEA-SM-227/98.
6. D. Gihwala and M. Peisach, J. Radioanal. Nucl. Chem. Lett., 106, (1986), p. 9.
7. I. Vickridge, J. Tallon and M. Presland, Nucl. Inst. and Meth. B, 85, (1994), p. 95.
8. S.M. Tang, T.H. Ong., M.G. Tan, K.K. Loh, C.H. Sow, B. Yuan and I. Orlic, Nucl. Inst. and Meth. B, 75, (1993), p. 383.
9. Á.Z. Kiss, I. Biron, T. Calligaro and J. Salomon, Nucl. Inst. and Meth.B, 85, (1994), p. 118.
10. P.H. Stelson, J.K Dickens, S. Raman and R.C. Trammall, Nucl. Inst and Meth., 98, (1965), p. 481.
11. C. Chasman, K.W. Jones and R.A. Ristinen, Nucl. Inst. and Meth., 37, (1965), p. 1.
12. G. Deconnick, Introduction to Radioanalytical Physics, Akadémiais Kiadó, Budapest, (1978).

FACULTY SPONSOR

Dr. Árpád Zoltán Kiss
Institute of Nuclear Research of the Hungarian Academy of Sciences
Department of Nuclear Physics
18/c Bem tér
Debrecen, Hungary, 4028
azkiss@atomki.hu

RELATIVISTIC PENDULA

Eric Jones
Department of Physics and Astronomy
University of Southern Mississippi
Hattiesburg, MS 39406-5046
received August 6, 1997

ABSTRACT

We solve for the angular motion of the relativistic simple pendulum driven by uniform driving forces of two distinct types: gravity and a uniform electric field. In both cases, we calculate and plot the angular motion of the pendulum in time. We also find the period of the pendulum as a function of its amplitude. While these two relativistic pendula do not differ greatly in their motion, the motion of each type of relativistic pendulum differs significantly from the classical large amplitude pendulum. The classical and relativistic pendula differ greatly in the period vs amplitude characteristics. We also calculated the period of each type of pendulum in the non-inertial frame of the pendulum itself. For a given amplitude, the period in the non-inertial frame is less than that determined in the stationary frame.

INTRODUCTION

One of the basic mechanics problems than an undergraduate physics or engineering major learns to solve is the motion of a simple pendulum. [1] Initially, the pendulum problem is solved assuming that the amplitude is small, resulting in simple harmonic motion. Later on, the student learns to solve Newton's law determining the motion of the pendulum for arbitrary amplitude, [2] a nonlinear differential equation whose solution is found in terms of elliptic functions.

The solution of the generalization of Newton's second law to account for the relativistic motion of a pendulum requires no essentially new techniques, but the resulting equations are a bit difficult to solve than those for the classical case. There are two such pendula whose motions are distinguished from one another by the nature of the uniform force which drives the pendulum: a constant gravitational field interacting with the mass at the end of the pendulum or a constant electric field interacting with a charged mass at the end of the pendulum. In both cases, one can find the period of the pendulum as a function of the proper amplitude by reducing the equations of motion to quadrature. This can be done both in a stationary inertial reference frame and the non-inertial reference frame of the pendulum mass itself.

Eric is a senior physics major at the University of Southern Mississippi. This research was begun during his Junior year. He is currently finishing up his last semester of study for the bachelor's degree in physics. He is considering graduate work in physics next year. In his very skimpy spare time, he can be found skateboarding and playing Dungeons and Dragons.

EQUATION OF MOTION OF THE RELATIVISTIC PENDULUM.

A plane simple pendulum of mass m, carrying charge q, is supported by a massless rod of proper length , L as shown in Figure 1. The pendulum is released from rest with respect to a fixed support (the origin of the inertial reference frame 'O') from angular position $\theta(0) = A$ as measured from the vertical. $\vec{W}(v)$ is a spatially uniform force in 'O' in the $-\hat{y}$ direction.

In reference frame 'O', Newton's second law is

$$\frac{d}{dt}(m\,\vec{v}\,\gamma) = \vec{T} + \vec{W}(v)\ , \qquad (1)$$

where $\vec{T}$ is the tension in the rod and

$$\gamma = \frac{1}{\sqrt{1 - v^2/c^2}}\ . \qquad (2)$$

Taking the derivative in equation 1 and taking the cross product of each term in Equation 1 with $\vec{r}$, the position of the mass with respect to the origin of the 'O' reference frame yields:

$$m\gamma\ \vec{r}\times\dot{\vec{v}} + m\gamma\,\vec{r}\times\ddot{\vec{v}} = \vec{r}\times\vec{W}(v)\,, \qquad (3)$$

where the overdot denoted differentiation with respect to time. Since the tension in the rod is along the rod:

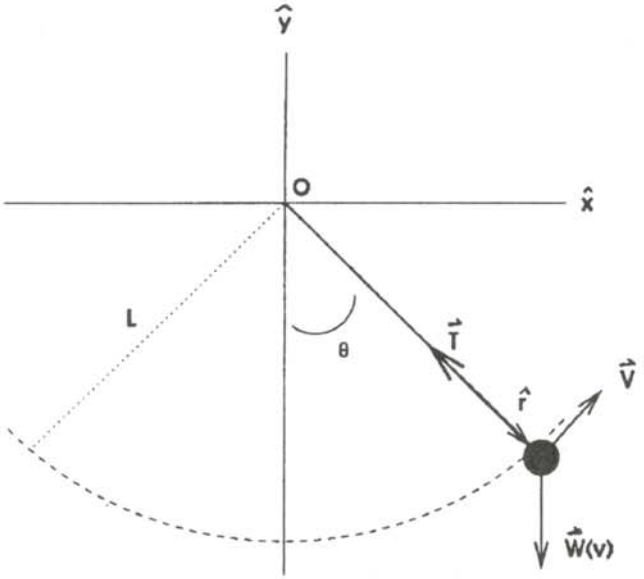

Figure 1
Schematic diagram of the pendulum showing the forces as determined in the inertial frame stationary with respect to the suspension point of the pendulum. The z direction points out of the diagram.

$$\vec{r} \times \vec{T} = 0 \ , \tag{4}$$

The remaining vector products are computed using the directions shown in Figure 1:

$$\begin{aligned} \vec{r} \times \vec{W}(v) &= -L\, W(v) \sin(\theta)\, \hat{z} \\ \vec{r} \times \left(m \gamma\ \vec{v}\right) &= m \gamma\ L v \hat{z} \\ \vec{r} \times \left(m \gamma \dot{\vec{v}}\right) &= m \gamma L \dot{v} \hat{z} \ , \end{aligned} \tag{5}$$

where $\hat{z}$ is the unit vector in the z-direction. The third equation in Equation 5 follows from the identity:

$$\vec{r} \times \dot{\vec{v}} = \frac{d}{dt}\left(\vec{r} \times \vec{v}\right) = \frac{d}{dt}\left(L v \hat{z}\right) \ . \tag{6}$$

Inserting Equation 5 into equation 3 yields:

$$v \dot{\gamma} + \gamma \dot{v} = -\frac{W(v)}{m} \sin(\theta) \ . \tag{7}$$

Differentiating Equation 2 with respect to time gives:

$$\dot{\gamma} = \frac{v \dot{v}}{c^2} \gamma^3 \ . \tag{8}$$

Putting Equation 8 into Equation 7 gives:

$$\gamma^3 \dot{v} = -\frac{W(v)}{m} \sin(\theta) \ . \tag{9}$$

To bring Equation 9 into a more standard form, the dependent variable is changed from $v(t)$ to $\theta(t)$. Since v is the tangential velocity of the mass, it is related to the angular position by:

$$v = L \dot{\theta} \quad \text{and} \quad v = L \ddot{\theta} \tag{10}$$

Substituting Equation 10 into Equation 9 :

$$\ddot{\theta} = -\frac{W(\dot{\theta})}{m L} \sin(\theta) \left(1 - \frac{L^2 \dot{\theta}^2}{c^2}\right)^{\frac{3}{2}} \tag{11}$$

We note in passing that Equation 11 reduces to the equation governing the non-relativistic pendulum as $v/c \to 0$ and the driving force replaced by $W = mg$.

It is convenient to introduce a dimensionless time variable:

$$\eta \equiv \frac{c\, t}{L} \tag{12}$$

Changing the variables according to Equation 12, Equation 11 becomes:

$$\frac{d^2\theta}{d\eta^2} = -\frac{L\, W\left(\frac{d\theta}{d\eta}\right)}{m c^2} \left(1 - \left(\frac{d\theta}{d\eta}\right)^2\right)^{\frac{3}{2}} \sin(\theta) \tag{13}$$

Equation 13 determines the motion of the pendulum in the reference frame 'O' due to an arbitrary driving force $W(v)$. While the equation is nonlinear, it is still an autonomous differential equation which can be reduced to quadrature by standard techniques. [4] We solve Equation 13 for the two special cases of the driving force and determine the angular motion and period in each case.

MOTION AND PERIOD

Motion

There are two distinct motions of the relativistic pendulum. The first type is driven by a uniform gravitational field. This field is effectively velocity dependent because the effective gravitational mass of the pendulum $E/c^2 = m\gamma$. Thus the driving force takes on the form:

$$\vec{W}(v) = m g \gamma (-\hat{y}) \tag{14}$$

The second type of relativistic pendulum is driven by a uniform, constant electric field, E. Because the total charge q is a Lorentz invariant scalar, this force does not depend on the speed of the pendulum. Ignoring any radiation due to the acceleration of the charged pendulum, the driving force becomes:

$$\vec{W}(v) = q E (-\hat{y}) \tag{15}$$

The equations of motion for each of these special cases follow from Equation 13 by inserting the appropriate form of the driving force (Equations 14 and 15). The gravity driven pendulum equation is denoted by *(G)* and the electric field driven pendulum equation by *(E)*:

$$\begin{aligned} \frac{d^2\theta}{d\eta^2} &= -\kappa \sin(\theta) \left(1 - \left(\frac{d\theta}{d\eta}\right)^2\right), \quad (G) \\ \frac{d^2\theta}{d\eta^2} &= -\kappa \sin(\theta) \left(1 - \left(\frac{d\theta}{d\eta}\right)^2\right)^{\frac{3}{2}}, \quad (E) \end{aligned} \tag{16}$$

where we have defined the constant κ by:

$$\begin{aligned} \kappa &= \frac{m g L}{m c^2} \quad (G) \\ \kappa &= \frac{q E L}{m c^2} \quad (E) \end{aligned} \tag{17}$$

To numerically solve Equation 16 for $\theta(\eta)$, we convert

these equations of motion to two systems of first-order differential equations:

$$\frac{d\theta}{d\eta} = \Omega,$$
$$\frac{d\Omega}{d\eta} = F(\theta,\Omega)\ , \qquad (18)$$

where the 'forcing function" , F(θ, Ω) is:

$$F(\theta,\Omega) = -\kappa \sin(\theta)\left(1-\Omega^2\right)\ ,\ (G)$$
$$F(\theta,\Omega) = -\kappa \sin(\theta)\left(1-\Omega^2\right)^{\frac{3}{2}}\ ,\ (E) \qquad (19)$$

The coupled first order differential equations, Equations 18 determining θ(η) were solved using the second-order Runge-Kutta approximation in MAPLEV™. [5] The numerical solutions for generated using this method are plotted in Figure 2. We chose the amplitude, A = 3 radians and the constant κ = 1 in both cases. The value of A = 3 radians corresponds to a very large initial amplitude, so even in the non-relativistic case, the equation of motion is nonlinear. Three cases for these initial parameters are shown in Figure 2, both driving forces in the relativistic case and the non-relativistic gravitationally driven pendulum. There is a significant difference between the relativistic and non-relativistic motion, but with the parameter κ = 1, there is not a great difference between the gravity driven and electric field driven relativistic pendula over the entire period of the motion.

Period

The equations of motion, Equations 16, are autonomous differential equations, the independent variable is not

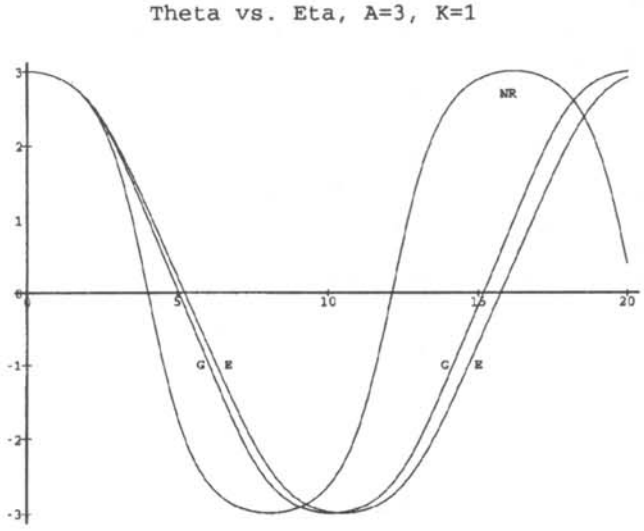

Figure 2

Angular position (in radians) of the pendulum vs time: non-relativistic, (NR); relativistic gravity driven, (G); relativistic electric field driven, (E). The horizontal axis is the dimensionless time η = ct/L. This time is that determined with respect to a stationary inertial frame.

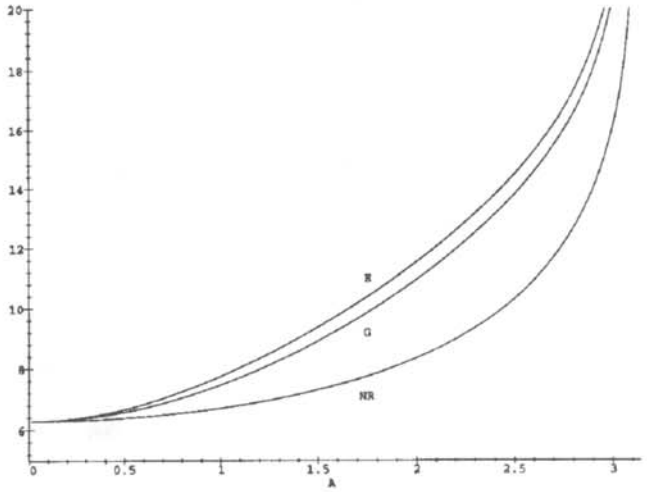

Figure 3

Period of the pendulum vs amplitude: non-relativistic, (NR); relativistic gravity driven, (G); relativistic electric field driven, (E). The vertical axis is the dimensionless period that is determined with respect to a stationary inertial frame.

explicit. Thus, we make a change of the dependent variable:

$$\Omega(\theta) = \frac{d\theta}{d\eta}\ ,$$
$$\frac{d^2\theta}{d\eta^2} = \frac{d\Omega}{d\eta} = \frac{d\Omega}{d\theta}\frac{d\theta}{d\eta} = \Omega\frac{d\Omega}{d\theta}\ , \qquad (20)$$

In this new dependent variable, the Equations 16 become:

$$\Omega\frac{d\Omega}{d\theta} = -\kappa \sin(\theta)\left[1-\Omega^2\right]\ ,\ (G)$$
$$\Omega\frac{d\Omega}{d\theta} = -\kappa \sin(\theta)\left[1-\Omega^2\right]^{\frac{3}{2}}\ ,\ (E) \qquad (21)$$

Equations 21 are separable and thus may be integrated. Recalling the initial conditions θ(0) = *A* and Ω(θ(0)) = 0, we obtain for the first integral:

$$\frac{d\theta}{d\eta} = \Omega = -\sqrt{1-\exp\left[2\kappa\left\{\cos(A)-\cos(\theta)\right\}\right]}\ ,\ (G)$$
$$\frac{d\theta}{d\eta} = \Omega = -\sqrt{1-\left[1+\kappa\left\{\cos(\theta)-\cos(A)\right\}\right]^{-2}}\ .\ (E) \qquad (22)$$

The period, *P*, is obtained by one more integration of Equations 22:

$$P = 4\int_0^A \frac{d\theta}{\sqrt{1-\exp\left[2\kappa\left\{\cos(A)-\cos(\theta)\right\}\right]}}\ ,\ (G)$$

$$P = 4\int_0^A \frac{d\theta}{\sqrt{1-\left[1+\kappa\left\{\cos(\theta)-\cos(A)\right\}\right]^{-2}}}\ ,\ (E) \qquad (23)$$

The integrals in Equations 23 were evaluated using Gaussian quadrature. [6] Figure 3 is a plot of the period obtained from Equations 23 for each type of pendulum for a range of amplitudes from 0 to 3 radians and a value of $\kappa = 1$. For comparison, we also plot period for the same amplitude ranges for the non-relativistic pendulum. The period, P, does not differ greatly between the two types of relativistic pendula, but the periods of these two pendula do differ from the period of the classical pendulum with the same amplitude. In both relativistic cases, the period is somewhat larger than the classical value. This is the case ecause the effective relativistic mass is greater than its classical couinterpart.

Period in the Reference Frame of the Pendulum Bob

The period values thus far calculated are those determined by observers at rest with respect to the pendulum support, reference frame 'O'. It is possible to calculate the period as determined by observers who are riding in the non-inertial reference frame of the pendulum mass itself. This calculation is accomplished by working in an inertial reference frame which is moving instantaneously with the pendulum mass at some fixed instant of time. An infinitesimal interval of time in this frame is related to the infinitesimal interval of time in the 'O' frame by:

$$d\tau = \frac{dt}{\gamma} = \sqrt{1 - \frac{v^2(t)}{c^2}}\, dt\,, \qquad (24)$$

where $v(t)$ is the instantaneous velocity of the pendulum in the 'O' frame. Changing the variable as defined in Equation 20, dimensionless proper time, $d\sigma$, becomes:

$$d\sigma = \sqrt{1 - \Omega^2(\eta)}\, d\eta = \sqrt{1 - \Omega^2(\theta)}\, \frac{d\theta}{\Omega}\,. \qquad (25)$$

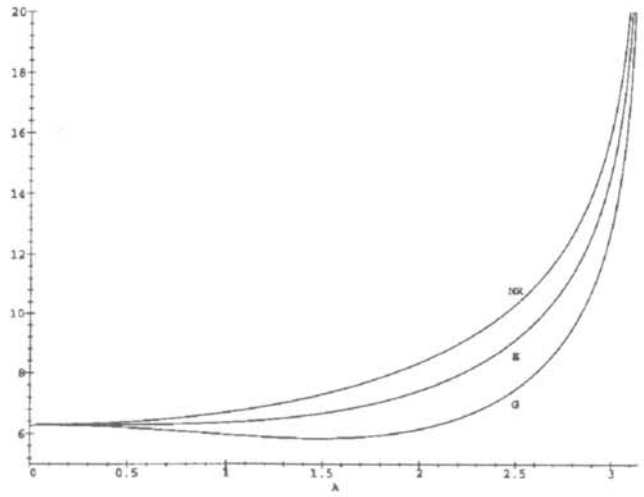

Figure 4
Period of the pendulum vs amplitude: non-relativistic, (NR); relativistic gravity driven, (G); relativistic electric field driven, (E). The vertical axis is the dimensionless period that is determined with respect to the non-inertial frame of the pendulum mass.

The period in the frame of the pendulum can now be found by integrating Equation 25 with respect to the variable θ. Explicit expressions for $W(\theta)$, given in Equations 22, are substituted into Equation 25, resulting in:

$$P = 4\int_0^A \frac{\exp\left[\kappa\,\{\cos(A) - \cos(\theta)\}\right]}{\sqrt{1 - \exp\left[2\,\kappa\,\{\cos(A) - \cos(\theta)\}\right]}}\, d\theta, \quad (G)$$

$$P = 4\int_0^A \frac{d\theta}{\sqrt{\left[1 + \kappa\,\{\cos(\theta) - \cos(A)\}\right]^{-2} - 1}}\,. \quad (E) \qquad (26)$$

The integrals in Equations 25 were again evaluated using Gaussian quadrature and the numerical results plotted in Figure 4. The curves represent the period vs amplitude lie well below the corresponding curves for the non-relativistic pendulum. The two period curves, derived from the different driving forces, are somewhat more separated than the corresponding curves determined for the inertial frame 'O'.

SUMMARY

We have extended the concept of the simple plane pendulum into the relativistic domain. There are two distinct forms of the simple plane pendulum as distinguished by the nature of the force that drives the pendulum. The difference arises because the gravitational driving force is velocity dependent, while the electric driving force is independent of velocity. We solve the equations of motion numerically and calculated the amplitude dependence of the period of each pendulum type in both an inertial frame and in a reference frame moving with the pendulum.

The solution of the relativistic pendulum required no essentially new techniques. The resulting equations are only a bit more difficult to solve than those in the classical case. It surprised us somewhat that we were unable to locate the explicit solutions to the angular motion of the relativistic pendulum. A literature search revealed explicit solutions of the equation of motion for the relativistic simple harmonic oscillator in one dimensions [7,8] which is one component of the two-dimensional motion of the plane pendulum. However, we did not find an explicit solution for the angular motion of such a plane relativistic pendulum. We also found that there remains considerable interest in the pendulum in both relativistic and general relativistic contexts. [9]

ACKNOWLEDGMENTS

The author would like to thank Dr. Lawrence Mead for his guidance in research, as well as his advice on the proper paper writing techniques. This work was supported in part by the NASA Space Grant College and Fellowship Program, under Grant No NASA NGT-40028.

REFERENCES

1. D. Halliday, R. Resnick and J. Walker, Fundamentals of Physics, 5th Ed. (Wiley,), 1997, pp. 381-384.
2. J. Marion and S. Thornton, Classical Dynamics of Particles and Systems, 4th Ed. (Saunders Publishing), 1995, pp. 162-167.
3. H.F. Goldstein and C.M. Bender, J. Math. Phys., 27, (1986), pp. 507-511. A similar dichotomy was found by Bender and Goldstein in the solution of the relativistic Bachistrochrone problem. A particle falling in a uniform gravitational field has a different minimum-time curve to move between two fixed points than a particle "falling" in a uniform electric field.
4. C.M. Bender and S. Orzag, Advanced Mathematical Methods for Scientists and Engineers, (McGraw-Hill, NY), 1978, Ch. 4.
5. J. Mathews and R.L. Walker, Mathematical Methods of Physics, 2nd Ed., (W.A. Benjamin, Inc.), 1970, ch. 13.
6. *Ibid*., Ch. 13.
7. A.L. Harver, Phys. Rev. D, 6, (1972), p. 1474-1476.
8. L.A. MacColl, Am. J. Phys., 26, (1957), pp. 535-538.
9. There is still interest and application of the relativistic pendulum in the context of general relativity. An example is: Y.S. Kim and M.E. Noz, Am. J. Phys., 46, (1978), pp. 480-482. More recently, the relativistic pendulum has appeared in the context of gravitational measurements: V.B. Braginsky, A.G. Polnarev and K.S. Thorne, Phys. Rev. Lett., 53, (1984). pp. 863-866; and radiation theory in: V.A. Balakirev, V.A. Buts, A.P. Tolstolushskii and Y.A. Turkin, Ukrainian J. of Physics, 28, (1983), pp. 1644-1647. Also, an interesting proposal concerning dual mass types and involving the relativistic pendulum has appeared in: W. Cates, A Cresswell and R.L. Zimmerman, Gen. Re. and Grav., 20, (1988), pp. 1055-1066.

FACULTY SPONSOR

Dr. Lawrence R. Mead
Department of Physics and Astronomy
University of Southern Mississippi
Hattiesburg, MS 39406-5046
lrmead@whale.st.usm.edu

ELECTRODEPOSITION OF $Cu_XIn_{2-X}Se_2$ THIN FILM JUNCTIONS

David M. Palacios * and Phillip C. Kalmanson †
Department of Physics and Space Science
Florida Institute of Technology
Melbourne, FL 32901-6988
received June 12, 1997

ABSTRACT

The electrochemical deposition of polycrystalline thin film junctions based on the $Cu_XIn_{2-X}Se_2$ system (CIS) was investigated We deposited separate *p*-type and *n*-type thin films and a *pn* junction from a single aqueous solution by varying the deposition potential. The films were examined with a scanning electron microscope; the stoichiometry determined by energy dispersive spectroscopy. The crystal structures of the films were determined using X-ray diffraction. The ability to deposit a thin film *pn* junction diode from the same single aqueous solution was verified by measuring current vs. voltage characteristics for both Ohmic and rectifying contacts to *n*-type $Cu_XIn_{2-X}Se_2$ and the *pn* junction. The current vs. voltage graphs made from the CIS thin film *pn* junction showed rectifying behavior, demonstrating our ability to make a *pn* junction from a single solution.

INTRODUCTION

$Cu_XIn_{2-X}Se_2$ (CIS) has been investigated for use as a thin film photovoltaic material due to its favorable optical bandgap and electrical properties. [1] CIS is a very good absorber over a wide range of photon energies and is also a good electrical conductor. Electrochemical deposition or electrodeposition is an inexpensive alternative to the more common high vacuum methods used to grow polycrystalline CIS thin films. Electrodeposition provides potentiostatic (constant voltage over a varying current) control of stoichiometry and is easily scalable from small to large area.

David is a first year graduate student enrolled in the doctoral program at Worcester Polytechnic Institute, where he is a teaching assistant. This research was completed as an undergraduate at Florida Institute of Technology. He is currently doing research in nonlinear optics. He hopes to apply nonlinear optical systems to electro-optical devices. His other research interests include semiconductor devices and laser manipulation of small particles. Outside the lab, his hobbies include Wah Lum Kung Fu, hiking and writing.

Phillip is currently a senior in physics at the Florida Institute of Technology. He is still pursuing research into copper indium diselenide thin films by participating in the construction of a space shuttle payload that will grow these films in space during the summer of 1998. His other research involves building an imaging Fourier transform spectrometer based on a Mach-Zehnder interferometer. He plans to attend graduate school and enter into a doctoral program in gravitation.

CIS acts as a *p*-type semiconductor if the ratio of Cu to In is greater than 1 (or $X > 1$) and acts as a *n*-type semiconductor if the ratio of Cu to In is less than 1 (or $X < 1$). If the value of X can be varied by the potential difference as the film is deposited, then one could made a *pn* junction by using a voltage step function.

The current vs. voltage behavior of a *pn* junction is to conduct when the potential difference is in one direction (forward bias) and not when it is in the other direction (reverse bias). This is commonly called a rectifying or diode behavior. A similar behavior, known as a Schottky barrier, can be produced when a metal is placed in contact with a semiconductor. If the work function of the metal is greater than the work function of the *n*-type semiconductor, the junction exhibits diode behavior. However, if the work function of the metal is less than the work function of the n-type semiconductor, the contact will display Ohmic behavior. The Schottky behavior is reversed for p-type films.

THE EXPERIMENT

The electrochemical deposition solution was prepared by dissolving various inorganic salts and a suitable

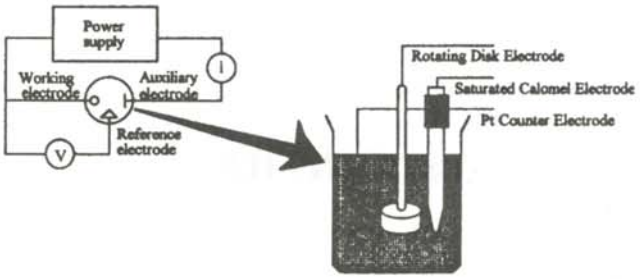

Figure 1
Schematic diagram of the electrochemical deposition and the cell.

complexing agent into doubly deionized water. These salts disassociated and introduced the desired ions into the aqueous solution. Our deposition bath consisted of a 10mM $In_2(SO_4)_3$, 5mM SeO_2, 1mM $CuSO_4$ and 25mM trisodium salt dihydrate (sodium citrate) solution. This solution, when prepared at room temperature, was light blue in color with a pH of 3.4. The solution was stirred for a minimum of 24 hours before the depositions were performed. The substrates used were either mechanically polished molybdenum discs or commercially obtained indium tin oxide (ITO) coated glass. The substrates acted as the working electrode in our electrochemical cell and were rotated at 400 r.p.m. during deposition. The rotation was used to circulate the solution and insure a uniform concentration of ions at the electrode surface.

The electrochemically deposited thin films were synthesized using a three electrode cell shown in Figure 1. We applied a potential between the substrate, or working electrode, and a platinum counter electrode placed in the deposition solutions. A saturated calomel electrode (SCE) was used to reference the potentials. The deposition potentials were created and monitored by a Keithley 236 Source/Measurement Unit which was interfaced with a personal computer and an EG&G 362 Scanning Potentiostat. An EG&G 212 Rotating Disk Electrode unit was used to control the rotation rate of the working electrode.

Deposition over-potentials for various ions in the solution were determined by cyclic voltammetry. This was done by sweeping the voltage across the cell and measuring the current (see Figure 2). A sudden rise in the current indicated the deposition potential for each ion. The stoichiometry of the film being deposited will, therefore, be dependent on the deposition potential. [2] The ratio of Cu to In in CIS (or the value of *X*) in the films changes in a linear fashion in the potential range from -1.3 V to -0.9 V with respect to the SCE. [3] In this manner, we can determine if the film deposited is a *p*-type or *n*-type semiconductor film.

The thickness of the film, Λ, being deposited was determined using Faraday's law [4]:

$$\Lambda = \frac{1}{n F A}\left(\frac{i t M}{\rho}\right), \qquad (1)$$

where i is the current, t is the time the potential is applied, M is the formula weight of CIS (336.28 g/mole), ρ is the density of CIS (5.77 g/cm3) [5], A is the area of the substrate exposed to the solution, F is Faraday's number, and n is the number of electrons transferred. The number of electrons, n, was taken to be 13 according to the reaction:

$$Cu^{2+} + In^{3+} + 2\,SeO_3^{2-} + 12\,H^+ + 13\,e^- \rightarrow CuInSe_2 + 6\,H_2O\,. \quad (2)$$

Depositions

The first deposition (A) to create an *n*-type thin film was deposited for 300 sec at a voltage of -1.3 V. The second deposition (B) to create a *p*-type thin film was deposited for 300 sec at -1.1 V. The films were deposited on a molybdenum substrate. The procedure was repeated for deposition times of 450 sec and 600 sec. The *pn* junction was made by depositing *n*-type CIS on a *p*-type CIS film which had been deposited onto an ITO coated glass substrate. For the creation of the *pn* junction, we just changed the over-potential by stepping the applied voltage during the continual growth of the thin film. For deposition on ITO coated glass, it was necessary to shift the over-

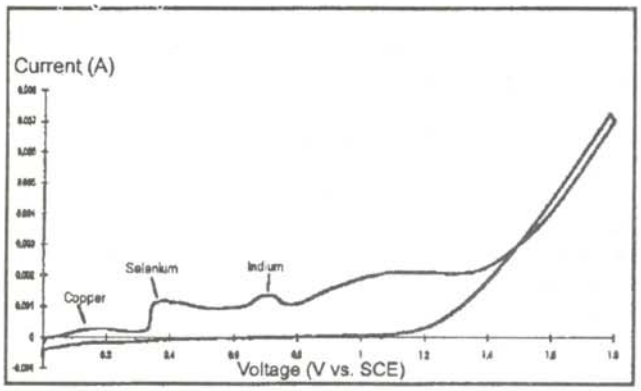

Figure 2
Cyclic voltammogram of our electrochemical bath used in this study. The peaks show the deposition potential for each ion.

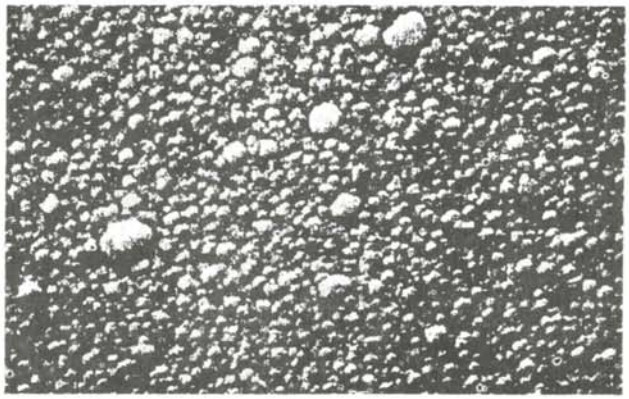

Figure 3
SEM micrograph of a 5 μmx 10μm CIS thin film surface.

	potential Volts	thickness microns	Stoichiometry	Cu/In	type
A	-1.3	0.59	$Cu_{1.04}In_{0.88}Se_{2.08}$	1.18	p
B	-1.1	0.69	$Cu_{1.07}In_{0.84}Se_{2.09}$	1.27	p
C	-1.3	1.00	$Cu_{0.94}In_{1.03}Se_{2.03}$	0.91	n
D	-1.1	0.88	$Cu_{1.14}In_{0.93}Se_{1.93}$	1.22	p
E	-1.3	1.20	$Cu_{0.94}In_{0.96}Se_{2.09}$	0.98	n

Table 1

Results of electron dispersive spectroscopy. The Cu/In ratio varied as anticipated with the exception of sample A. Sample A should have been n-type according to the potential used. Consequently, we used a more negative potential when making the n-type layer of the pn junction.

potentials used for molybdenum by -1.0V. When the pn junction was fabricated, the *p*-type CIS was deposited at -2.1 V and the *n*-type CIS deposited at -2.5V. The more negative value for the potential in this case was used to insure that the material was n-type (see Table 1).

DATA PRESENTATION AND INTERPRETATION OF RESULTS

SEM and EDS Film Characterization

A scanning electron microscope (SEM) was used to view the surface of the thin films. A SEM micrograph was made of the surface of our CIS deposited onto molybdenum (see Figure 3) This micrograph shows a dense homogeneous polycrystalline morphology. Using the SEM, we performed electron dispersive spectroscopy (EDS). In EDS, the sample is bombarded with high energy electrons. These electrons knock the inner orbital electrons out of the atoms, allowing an outer orbital electron to cascade into the inner vacancy. For the outer electron to make this transition, it emits a photon in the X-ray region. Since each atom emits its own characteristic photons, the stoichiometry of the sample can be determined by measuring the intensity and energy of the emitted X-rays. An example of the X-ray spectrum is shown in Figure 4. Table 1 shows the stoichiometry of our samples as determined by EDS.

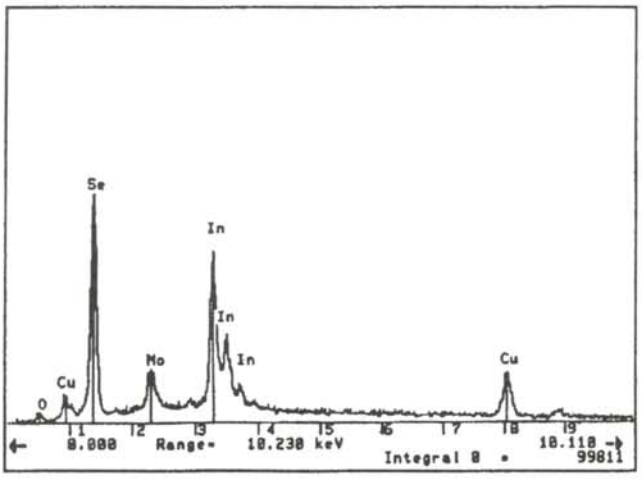

Figure 4

Electron dispersive spectroscopy scan showing the relative intensity of the characteristic X-rays versus the X-ray energy.

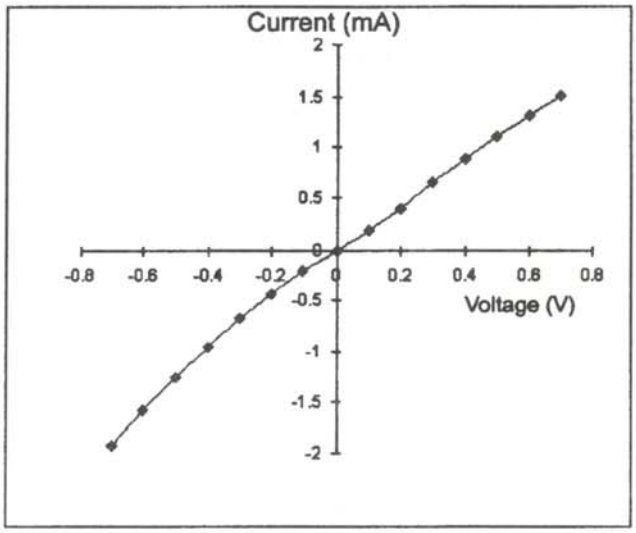

Figure 5

Current versus voltage behavior of a copper contact on an n-type CIS film indicating an Ohmic response.

X-ray Diffractometry

To determine the crystal structure of our films, we used X-ray diffraction (XRD). XRD is the diffraction of X-rays from the periodic arrangement of atoms in a crystal. We illuminated the sample with Cu K_α X-rays and measured the intensity of the diffracted beams as a function of the incident angle. [6]

CIS has previously been found to have the chalcopyrite crystal structure. [7] The experimentally determined XRD pattern, shown in Figure 5, of a 1 micron thick film deposited at -1.1 V is in good agreement with the theoretical XRD pattern for CIS.

I-V Measurements

The current vs voltage (*I-V*) characteristics of the junctions were done by ramping the voltage and monitoring the current. We tested our *I-V* measuring system using a commercial diode and resistor.

The *I-V* characteristics of a copper contact on the *n*-type CIS film, shown in Figure 5, were determined. This junction demonstrated the anticipated Ohmic behavior. This was done to insure that we were not observing false rectifying behavior caused by a Schottky barrier between our *pn* junction when using a copper contact on the *n*-side. A Schottky barrier was made by placing an aluminum contact on the *n*-type CIS film.

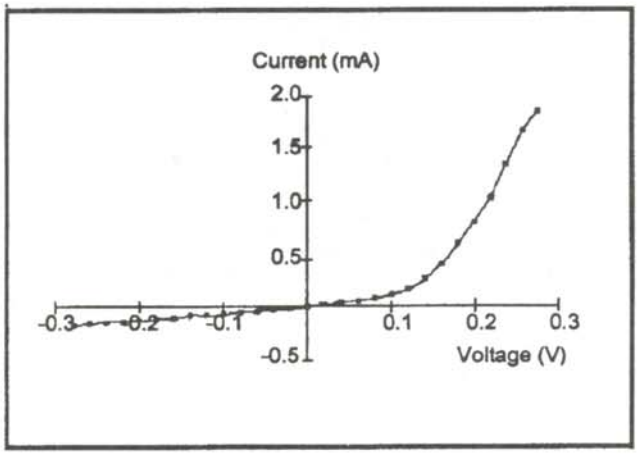

Figure 6
Current versus voltage behavior of a CIS pn junction. The diode type behavior indicated that we have successfully produced the pn junction.

The *I-V* characteristics for the *pn* junction are shown in Figure 6. These confirm the existence of the *pn* junction by verifying the anticipated rectifying behavior. Hence we demonstrated the ability to deposit a thin film *pn* junction diode from the same single aqueous solution during the continual growth of the thin film. This work supports the possibility of one day producing inexpensive photovoltaic solar cell materials.

ACKNOWLEDGMENTS

The authors would like to thank Dr. Raffaelle for giving us the opportunity to do this research. We would also like to thank graduate students Robert Freidfeld, Mehmet Argimitis and Hans Forsell for their assistance. We would like to acknowledge Eldar Noe for his help in our research efforts.

REFERENCES

* current address of the author: David M. Palacios, 152 West Street, 2nd floor, Worchester, MA, 01606.
† current address of the author: Phillip C. Kalmanson, 5404 Riddle Road, Holiday, FL, 34690.

1. A. Rockett and R.W. Birkmire, J. Appl. Phys., 70, (1991), p. R81
2. C. Guillen and J. Herrero, J. Appl. Phys., 71, (1992), P. 5479.
3. R.P. Raffaelle, J.G. Mantovani and R. Friedfeld, Solar Energy Materials and Solar Cells, in press.
4. D.S. Lashmore and M.P. Dariel, J. Electrochem. Soc., 135, (1988), p. 1218.
5. CRC Handbook of Chemistry and Physics, 71st Ed, (CRC Press, Inc.), Boston, 1990.
6. G. Burns, Solid State Physics, (Academic Press, Inc.), 1985.

FACULTY SPONSOR

Dr. Ryne P. Raffaelle
Department of Physics and Space Sciences
Florida Institute of Technology
Melbourne, FL 32901

PHASE TIME DETERMINATION FOR SUPERLUMINAL TUNNELING OF AN ELECTROMAGNETIC PULSE DURING FRUSTRATED TOTAL INTERNAL REFLECTION

Jeffrey Stuart Parker *
Department of Physics and Astronomy
Middle Tennessee State University
Murfreesboro, TN 37132
received July 10, 1997

ABSTRACT

We demonstrate that the use of the transmission line matrix modeling method is an effective technique for calculating the time-resolved response of two-dimensional structures to electromagnetic (EM) radiation. In particular, we examine the tunneling of EM radiation in a frustrated total internal reflection configuration. For such an event, we define and measure a "phase time" to represent the tunneling time of an EM pulse. Our simulations show that the pulse tunnels with superluminal velocity. The simulation also demonstrates that the phase times for these EM pulses are zero, independent of the thickness of the dielectric gap through which the pulse tunnels.

INTRODUCTION

This paper examines the use of transmission line matrix (TLM) as a technique for calculating the tunneling time of an electromagnetic (EM) pulse through a forbidden dielectric gap formed by a frustrated total internal reflections (FTIR) configuration (see Figure 1). The incident light wave hitting the bottom of the prism is at an angle such that, according to Snell's law, there is no transmitted wave. If a second prism is placed a finite distance away from the upper prism, a portion of the wave in the top prism will transmit through the 'forbidden region' and appear as an attenuated wave in the lower prism. The EM waves seem to tunnel through the dielectric barrier separating the two prisms.

The question of how long the tunneling process takes was raised in the early years of quantum mechanics. Since then, much of the theoretical work has centered around electron tunneling in quantum mechanics. There has been, however, some recent work devoted to electromagnetic tunneling [1-3], including measurement of superluminal tunneling through optical fibers. [4-7]. Relating such results to quantum mechanical tunneling of particles is warranted by the analogy between the Helmholtz wave equation and the time-independent Schrödinger equation. [8] The transmission of EM radiation as seen in FTIR is a well observed and noted occurrence.[9,10] The tunneling time of

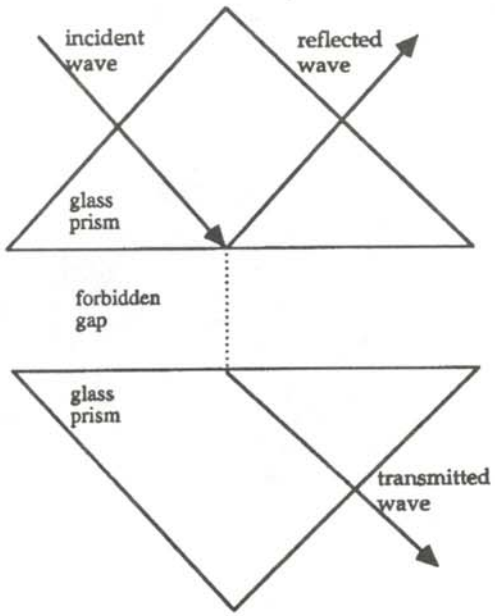

Figure 1
Representation of two-dimensional frustrated total internal reflections.

Jeff is a first year graduate student working in experimental condensed matter physics at Florida State University. This research was done during his final year at MTSU. In his spare time, he can be found trying to get in a few rounds of golf at the local Tallahassee courses or on one of the many Florida beaches.

this event, however, is not a completely resolved quantity.

PHASE TIME and GROUP VELOCITY

There have been several definitions presented for tunneling times. [2] We shall use the "phase time" definition: the time at which the peak of a tunneling wave packet emerges from the far side of a tunneling barrier relative to the time at which the peak of the incident wave packet enters the near side of the tunneling barrier. In some instances (our case), this may lead to a time less than the thickness of the barrier divided by the speed of light. This implies that the tunneling wave packet has a superluminal velocity, traveling faster than the speed of light, within the barrier.

This result has lead to skepticism over the validity of such a representation for the tunneling time. [11] However, the definition of group velocity:

$$v_g = \frac{d\omega}{dk} = \frac{c}{n + \omega \frac{dn}{d\omega}}, \qquad (1)$$

is now well understood to be a valid representation of the propagation of the peak of a wave packet. In regions of anomalous dispersion ($dn/d\omega < 0$), the group velocity can exceed the speed of light in a vacuum. There is no violation of causality or special relativity because the velocity of the energy is always less than c. [12-14]

TRANSMISSION LINE MATRIX METHOD

The Transmission Line Matrix (TLM) technique is an effective method for simulating the propagation of EM pulses through various dielectric arrays. It is based on a discrete form of Huygen's wave model in two-dimensional space and time. In this model, space is represented by a mesh of orthogonal transmission lines forming a Cartesian matrix of points or 'nodes', separated by a distance L. The simulation advances in discrete time steps

$$\Delta t = \frac{L}{c}, \qquad (2)$$

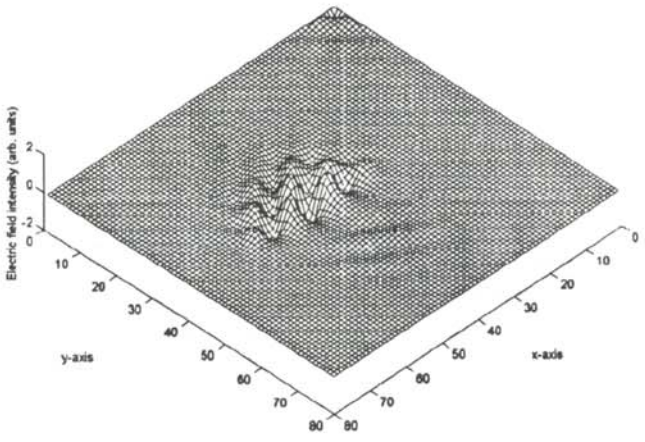

Figure 2
A surface plot of the electric field distribution for two-dimensional frustrated total internal reflections. The x-axis represents the electric field intensity.

where c is the speed of EM waves on the transmission line.

This two-dimensional model is an electrical network analog of EM wave propagation; the voltages and currents on the mesh representing the electric and magnetic fields of Maxwell's equations. The inductance and capacitance of these transmission lines mimic the permittivity and permeability of the vacuum. Small shunt stubs, called permittivity stubs, are located at the nodes of the mesh to simulate varying dielectric regions. The admittance of the stub:

$$y_o = 4\left(\varepsilon_r - 1\right), \qquad (3)$$

determines the dielectric constant of the mesh at that node. The stubs have length $L/2$ so that the signal will be reflected back from the end and arrive at the node at each time step Δt.

Initially, all of the voltage impulses on the mesh as set to zero. The mesh is then excited with input signals which can be entered at a selected group of nodes on the mesh. The propagation of the input signal through the mesh is achieved by calculating the voltage and current for each node at each time step. This is done by relating the incident voltage impulses at time $N\,\Delta t$ to the reflected impulses at time $(N+1)\,\Delta t$ via the matrix formula:

$$\begin{bmatrix} V_1 \\ V_2 \\ V_3 \\ V_4 \\ V_5 \end{bmatrix}_{N+1} = \frac{1}{2y} \begin{bmatrix} 1-y/2 & 1 & 1 & 1 & 1 \\ 1 & 1-y/2 & 1 & 1 & 1 \\ 1 & 1 & 1-y/2 & 1 & 1 \\ 1 & 1 & 1 & 1-y/2 & 1 \\ 1 & 1 & 1 & 1 & y_o-y/2 \end{bmatrix} \begin{bmatrix} V_1 \\ V_2 \\ V_3 \\ V_4 \\ V_5 \end{bmatrix}_N, \qquad (4)$$

where N is the time step index; $y = (4 + yo)$; V_1, V_2, V_3, and V_4 are the voltages on the four connected transmission lines; V_5 is the voltage on the permittivity stub. Because the matrix values are calculated at each time step, the TLM method can accurately simulate the temporal progression of the input signal. Hence, the analogs to the voltage and current: the electric and magnet fields respectively for a propagating EM are simulated. The simulator conveniently allows for a visual representation of the electric field on the mesh. The electric field distribution for FTIR is shown as a surface plot of the mesh in Figure 2.

The TLM method is easily programmed onto a digital computer and is able to evaluate complex problems in a relatively short period of time. The method is a well know technique for simulation of EM waves at microwave frequencies. It easily can be applied to optical frequencies when the simulated systems are purely dielectric (as they are in our case). Although the TLM simulator is a simple and effective method for calculating the propagation of EM pulses, it does have its limitations, such as mesh size and frequency response. [15] A more complete description of the TLM method can be found elsewhere. [16]

There exist commercial TLM packages, but most place

limitations on the mesh size. Since we needed to generate matrices (350 x 350 elements), we had to program our own simulator. It was written and operated in MATLAB™.

FTIR Simulation

The aim of this simulation was to model the effect of the tunneling an electromagnetic pulse through the forbidden gap of two dimensional frustrated total internal reflections. An example of the simulation configuration is shown schematically in Figure 3.

The dielectric constant of the tunneling gap is $\varepsilon_r = 1$ and the surrounding regions are of dielectric constant $\varepsilon_r = 6$ (index of refraction $n = 2.449$). This results in a critical angles less then 24°, considerably less than the 45° angle of incidence for the input wave packet. The mesh size was sufficiently large as to exclude interference from reflections of the input signal. To minimize the dispersion inherent in a finite wave train, the input nodes were chosen to be as close as possible to the tunneling barrier. Since the phase velocity is not the same for each frequency of the wave packet in a dispersive medium, we chose the input wave form to be Gaussian. This minimizes the uncertainty $\delta x\, \delta k$, where δx represents the length of the wave train and δk represents the spread in the wave number centered about some k_o.

The input time signal, shown in Figure 4, was obtained by generating a sinusoidal signal modulated by a Gaussian

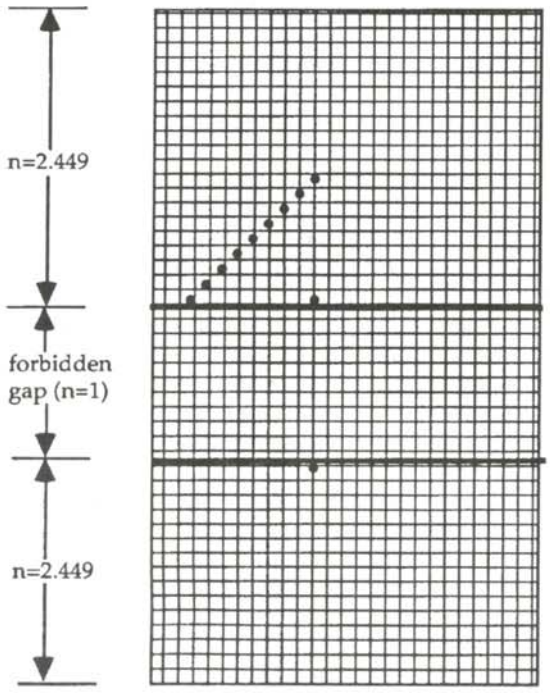

Figure 3
A schematic representation of the simulation mesh, showing the diagonal array of input points and the two output points on either side of the forbidden gap.

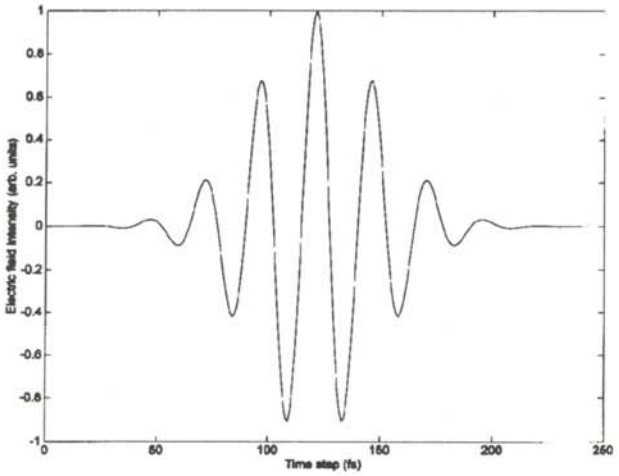

Figure 4
Input pulse: a sinusoidal signal modulated by a Gaussian envelope.

envelope:

$$s(t) = A \exp\left[i\, \omega_o\, t + \left(\frac{t}{t_o}\right)^2 \right], \qquad (5)$$

where ω_o is the center frequency and t_o is the time extent of the envelope. In the simulations presented here, t_o = 2.1 Fs and ω_o = 13 tHz.

To input this signal into the simulator, the real part of Equation 5 was sampled in discrete time intervals equal to the step time of the simulator. These values represent the electric field amplitudes used as signal inputs for each of the TLM input nodes. Nodes on either side of the tunneling barrier were chosen to be data outpoints (see Figure 3). The simulation was executed with four different barrier thicknesses (5, 10, 15 and 20 nodes). The voltage was recorded for each of the two output nodes after every time step.

Data taken from the output nodes show the propagation of the wave packet past output nodes. To find the phase time, we determined the time at which the peak of a tunneling wave packet emerged from the far side of the tunneling barrier relative to the time at which the peak of the incident wave packet interacted with the entrance side of the tunneling barrier. Since the two wave packets may not necessarily be in phase, the peak of the wave packet may be greater that the strongest local peak in one of the packets.. Therefore, we take the absolute magnitude of the wave packets. This is accomplished by performing a Hilbert transformation [17] on the wave packets. This changed the sinusoidal signal in time to the envelope of the wave packet.

Once we determined the time at which the peak of the input signal entered and emerged from the barrier, we calculated the phase time as the difference between these

two times. The simulation showed that the entrance and emergence of the signal peak, shown in Figure 5, was simultaneous for each tunnel thickness. We also determined the attenuation of the tunneling pulse by graphically representing the mesh inside the tunnel barrier as shown in Figure 6. The Gaussian form of the pulse is distinguishable and the expected attenuation of the signal intensity is present.

DISCUSSION AND RESULTS

Since the entrance and emergence of the peak of the wave packet are simultaneous for all four of the barrier thicknesses, we can infer that the phase time has a constant value of 0, independent of the thickness of the tunneling barrier. Such a phase time implies a superluminal group velocity for the tunneling signal inside the barrier. This results does not conflict with causality or special relativity as the large attenuation of the wave packet during tunneling insures in all cases that the velocity of the energy is less than the speed of light. Superluminal velocities have been predicted [4] and group velocities exceeding c have been experimentally observed in physical situations. These reports, in combination with the simulation results, demonstrate that for FTIR, an instantaneous phase time is a valid description for the tunneling time for an EM pulse.

ACKNOWLEDGMENTS

The author would like to thank his faculty research advisor, Dr. William Robertson, for the inspiration and guidance he provided. This work was performed at Middle Tennessee State University and was supported by grant number CC4115 from the Research Corporation.

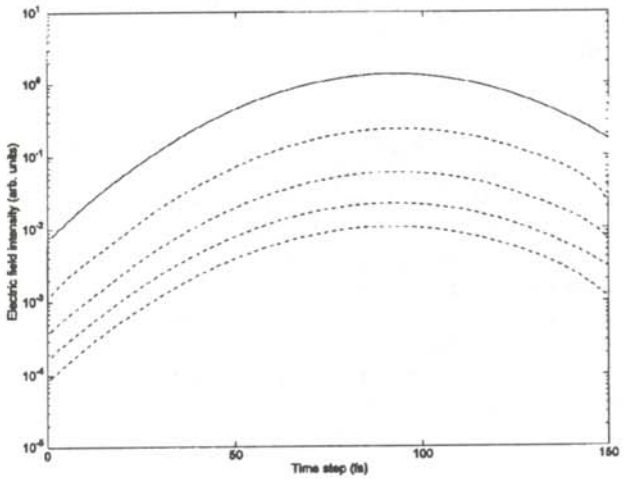

Figure 5

Log of the electric field intensity vs time at the entrance of the barrier (solid line) and at the exit of various barrier widths (dotted lines). The barrier gaps are 5, 10, 15, and 20 nodes wide. The intensity of the exit signal is shown to decrease with the barrier width.

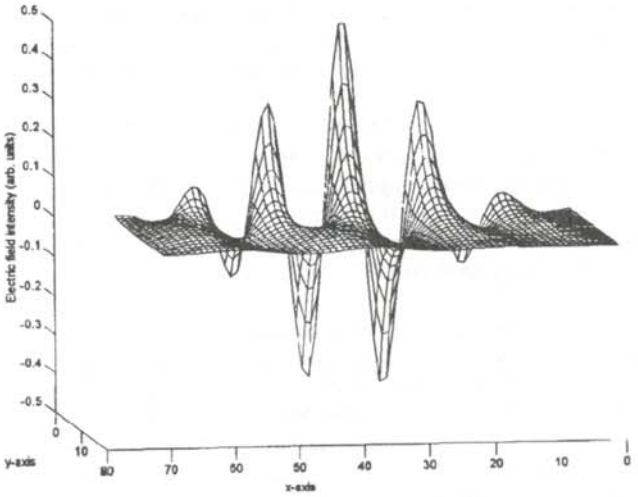

Figure 6

A surface plot of the electric field distribution within the forbidden region during two-dimensional frustrated total internal reflections. The z-axis represents the electric field intensity. The input signal form is clearly visible. The attenuation of the pulse as it tunnels through the barrier is well demonstrated.

REFERENCES

* Current address of the author: Jeff Parker, 253 Hayden Road, #254, Tallahassee, FL 32304.
1. M. Buttiker and R. Landauer, Phys. Rev. Lett., 49 (1982), p. 1739.
2. E.H. Hauge and J.A. Stovenberg, Rev. Mod. Phys., 61, (1989), p. 917
3. W. Jaworski and D.M. Wardlaw, Phys. Rev. A, 45, (1992), p. 2611.
4. W.M. Robertson, "Transmission Line Matrix Modeling of Superluminal Electromagnetic Pulse Tunneling Through the Forbidden Gap in Two-dimensional Photonic Band Structures", J. Opt. Soc. Am., 49, (1997), p. 1066.
5. C. Spielmann, R. Szipocs, A. Stingl and F. Krausz, "*Tunneling of Optical Pulses through Photonic Band Gaps*", Phys. Rev. Lett., 73, (1995), p. 2308.
6. A.M. Steinberg, P.G. Kwait and R.Y. Chiao, "*Measurement of Single-Photon Tunneling Time*", Phys. Rev. Lett., 71, (1993), p. 708.
7. A.M. Steinberg and R.Y. Chiao, "*Tunneling Delay Times and One and Two Dimensions*", Phys. Rev. 49, (1994), p. 3283.
8. A.M. Steinberg and R.Y. Chiao, Physica, 175B, (1991), p. 257.
9. W.C. Elmore and M.A. Heald, Physics of Waves, (McGraw-Hill), 1969, pp. 275-277.
10. B. Rossi, Optics, (Addison Wesley) 1957, pp. 379-387.
11. J.D. Jackson, Classical Electrodynamics, (Wiley), 1975, p. 302.

12. C.G.B. Garret and D.E. McCumber, "*Propagation of a Gaussian Light Pulse Through an Anomalous Dispersion Medium*", Phys. Rev. A., 1, (1970), p. 305.
13. M.D. Crisp, "Concept of Group Velocity in Resonant Pulse Propagation", Phys. Rev A.. 4, (1971), P. 2104.
14. S. Chu and S. Wong, "*Linear Pulse Propagation in an Absorbing Medium*", Phys. Rev. Lett., 48, (1982), p. 738.
15. W.M. Robertson, S.A. Boothroyd and L.Chan, "*Photonic Band Structure Calculations Using a Two-dimensional Electromagnetic Simulator*", Journal of Modern Optics, 41, (1994), p. 285.
16. W.J. Hoefer and P.P.M. So, The Electromagnetic Wave Simulator, (Wiley), 1991.
17. J.N Pandey and M.A. Chaudhry, "The Hilbert Transform of Generalized Functions and Applications", Canadian Journal of Mathematics, 35, (1983)

FACULTY SPONSOR

Dr. William Robertson
Department of Physics and Astronomy
Middle Tennessee State University
Murfreesboro, TN 37132
wmr@physics.mtsu.edu

DELTA EXPANSION FOR ENERGY LEVELS OF THE ANHARMONIC OSCILLATOR

Alex Gittings *
Department of Physics and Astronomy
University of Southern Mississippi
Hattiesburg, MS 39406-5046
received August 6, 1997

ABSTRACT

The δ-expansion was used to predict the quantum mechanical energy levels for potential energy of the form $V(x) = 1/2\, x^2 + \lambda\, x^p$, where $p = (2 + 2\delta)$. When $\delta = 1$ or $\delta = 2$, the anharmonicity is quartic and octic respectively. The anharmonic term in the potential energy is expanded in powers of δ. Perturbation theory in powers of δ was used to find the energy levels.. For the octic case, Padé summation was used to re-sum the δ-series which appeared to be diverging. Numerical results are compared with known exact results from the literature; errors range from theths of a percent to several percent.

INTRODUCTION

In quantum mechanics, an important problem is to solve for the energy eigenvalues, En, that are determined by Schrödinger's equation:

$$-\frac{\hbar^2}{2m}\frac{d^2\psi_n(x)}{dx^2} + V(x)\,\psi_n(x) = E_n\,\psi_n(x)\,, \qquad (1)$$

where $V(x)$ is the potential energy of a particle of mass m. There are very few potentials for which Schrödinger's equation can be solved for E_n exactly. Thus, it is necessary to develop approximate methods for finding energy eigenvalues for cases that cannot be solved exactly.

One common standard method for obtaining approximate eigenvalues is the Rayleigh-Schrödinger perturbation method in which one seeks to expand the energy eigenvalues and wavefunctions in terms of a small parameter. For example, consider the potential:

$$V(x) = \frac{1}{2}\, m\, \omega^2\, x^2 + g\, x^p\,. \qquad (2)$$

when $g = 0$, this reduces to the potential for a harmonic oscillator (for which the exact solutions are known). For small values of g, the energy eigenvalues and eigen functions are expanded in a series in powers of g. [1,2] It is known, however, that the power series that are developed for the energy eigenvalues for the potential in Equation 2 diverge for all values of g, no matter how small. [3]

Recently, new attempts have been made to find approximate solutions to difficult equations involving nonlinear (or non-quadratic) terms such as the anharmonic term One such attempt is the δ-expansion. [4] In this technique, the nonlinear terms are expanded in a parameter, δ, which, in effect, measures the degree of nonlinearity of the expanded term. In our case, the anharmonic term in Schrödinger's equation is the term which can be generalized to be:

$$g\, x^{(2+2\delta)}\,. \qquad (3)$$

When $\delta = 0$, this term reduces to the potential energy for a harmonic oscillator. When $\delta = 1$, the term becomes a quartic potential, when $\delta = 3$, the term becomes an octic potential. Thus, the parameter δ measures the deviation of the anharmonic potential from harmonicity.

The energy eigenvalue with this form for the anharmonic term will have an expansion similar to that of standard perturbation theory:

$$E_n = E_n^{(0)} + \delta\, E_n^{(0)} + \delta^2 E_n^{(0)} + \ldots \qquad (4)$$

The zeroth order term, $E_n^{(0)}$ is found by solving the simple harmonic oscillator problem. The corresponding wavefunction, $\psi_n^{(0)}$, is determined exactly in terms of the

Alex is a senior studying physics at the University of Arizona in Tuscon. He will graduate in December of 1998 with a degree in Engineering Physics. He plans to study particle physics in graduate school. The current research was performed during the summer of his junior year under a NASA Space Grant Summer Fellowship at the University of Southern Mississippi. In his spare time, he likes to hike, read and play racquet ball and chess.

Hermite polynomials. [1]. The higher order terms, $E_n^{(m)}$, $m = 1,2,...$ can, in principle, be found to any desired order from stand perturbation theory by expanding the anharmonic term in the potential in powers of δ.

DELTA EXPANSION FOR THE ENERGY EIGENVALUES

Schrödinger's Equation (Equation 1) and the potential energy (Equation 2) can be written in terms of dimensionless variables by making the substitution:

$$x = \sqrt{\frac{\hbar}{m\,\omega}}\; y\,. \tag{5}$$

Equation 1 becomes:

$$-\frac{1}{2}\frac{d^2\psi_n(y)}{dy^2} + \frac{1}{2}\,y^2\,\psi_n(y) + \lambda\, y^p\psi_n(y) = \bar{E}_n\,\psi_n(y), \tag{6}$$

where

$$\lambda = g\,\frac{\hbar}{4\,m^2\,\omega^3} \text{ and } \bar{E}_n = \frac{E_n}{\hbar\,\omega}\,. \tag{7}$$

Replacing p in the anharmonic terms with $(2 + 2\delta)$ and then expanding it in terms of δ gives:

$$y^{(2+2\delta)} = y^2\left\{1 + \delta\,\ln(y^2) + \frac{\delta^2}{2!}\left[\ln(y^2)\right]^2 + ...\right\}. \tag{8}$$

Substituting Equation 8 into Equation 6 gives:

$$2\,\bar{E}_n\,\psi_n(y) = -\frac{d^2\psi_n(y)}{dy^2} +$$

$$y^2\left\{1 + 2\lambda + 2\lambda\delta\,\ln(y^2) + \frac{\delta^2}{2!}\left[\ln(y^2)\right]^2 + ...\right\}\psi_n(y)\,. \tag{9}$$

It is convenient to normalize the coefficient of the y^2 term. This is done by substituting:

$$y = \frac{z}{\left(1 + 2\,\lambda\right)^{\frac{1}{4}}} \tag{10}$$

into Equation 9 to yield:

$$-\frac{d^2\psi_n(z)}{dz^2} + z^2\psi_n(z) + \delta\,f_1(x)\psi_n(z) + \delta^2 f_2(x)\psi_n(z) + ...$$

$$= \frac{2\bar{E}_n}{\sqrt{1 + 2\lambda}}\psi_n(z)\,, \tag{11}$$

where

$$f_1(z) = \frac{\lambda}{\frac{1}{2} + \lambda}\,z^2\,\ln\left[\frac{z^2}{\sqrt{1 + 2\lambda}}\right], \tag{12}$$

and

$$f_2(z) = \frac{1}{2}\,f_1(z)\,\ln\left[\frac{z^2}{\sqrt{1 + 2\lambda}}\right]. \tag{13}$$

We now want to find an expansion for the dimensionless energy in δ as in Equation 4:

$$\bar{E}_n \approx E_n^{(0)} + \delta\,E_n^{(1)} + \delta^2\,E_n^{(2)} + \delta^3\,E_n^{(3)}\,. \tag{14}$$

The zeroth order term in the expansion corresponds to the energy eigenvalues of the simple harmonic oscillator:

$$E_n^{(0)} = \sqrt{1 + 2\lambda}\left(n + \frac{1}{2}\right). \tag{15}$$

The normalized zeroth order wavefunction in terms of the Hermite Polynomials is:

$$\psi_n^{(0)}(z) = \frac{1}{\pi^{\frac{1}{4}}\sqrt{2^n n!}}\,H_n(z)\,\exp\left(\frac{z^2}{2}\right). \tag{16}$$

The first and second order coefficients in the expansion for the energy are:

$$E_n^{(1)} = <\psi_n^{(0)}(z)\,|\,f_1(z)\,|\,\psi_n^{(0)}(z)>\,, \tag{17}$$

and

$$E_n^{(2)} = <\psi_n^{(0)}(z)\,|\,f_2(z)\,|\,\psi_n^{(0)}(z)> +$$

$$\sum_{m\neq n}\frac{\|<\psi_n^{(0)}(z)\,|\,f_1(z)\,|\,\psi_n^{(0)}(z)>\|^2}{E_n - E_m}\,. \tag{18}$$

The third order term was found in terms of $\psi_n^{(0)}(z)$, $f_1(z)$, $f_2(z)$ and $f_3(z)$. [2] The detailed expressions for the third order perturbation energy are omitted for brevity. In the second order, 24 terms in the sum were sufficient to produce an accuracy of a few significant digits. In the third order, a double sum is necessary. To do this, 64 terms had to be evaluated. All integrals involved in the sums were performed using the symbolic program MAPLEV™.

RESULTS

Table 1 shows the exact energy eigenvalues obtained by standard configuration mixing, [5] and the corresponding energy values given by third-order deltaa expansion (δ = 1) for the ground, first and second excited states. Three separate values of λ are considered: λ = 0.1, 1.0 and 10.0. Larger values of λ tend to decrease the accuracy obtained from third order δ-expansions. This is not surprising since larger values of λ will make the anharmonic term more dominant when compared to the harmonic term. For λ =

State	λ	Exact	$\bar{E}$	% error
Ground	0.1	0.559146	0.555099	.72
	1.0	0.803771	0.807072	.41
	10.0	1.504972	1.981946	32
First	0.1	1.769503	1.764772	.27
	1.0	2.737892	2.712452	.93
	10.0	5.321608	6.465102	21
Second	0.1	3.138862	3.131423	.24
	1.0	5.179292	4.927973	4.9
	10.0	10.34706	11.21634	8.4

Table 1

A comparison of the exact energy values (reference 5) with energy values determined from third order δ-expansion for the ground, first and second excited states of the quartic anharmonic potential.

0.1 and 1.0, the errors are less than 1%. For $\lambda = 10.0$, less accuracy was obtained: the errors range from 8 % to 32% of the exact values.

Table 2 shows the individual terms of Equation 14 for the energy of the ground state of the octic oscillator. For both cases considered, $\lambda = 0.1$ and 1.0, the higher order terms in δ seem to diverge from the exact energy values. This was not the case for the quartic potential where the energy values for the ground and first two excited states approached the exact energy value as higher order terms were considered. Padré summation, which essentially rewrites the right hand side of Equation 14 as a ratio of polynomials, [7] can be used in this case to determine the energy eigenvalues.

Table 3 shows three Padé summations, ${}_1P_1$, ${}_2P_1$ and ${}_1P_2$. The subscripts indicate the orders of the polynomials (in δ) contained in the Padé representation. For example, ${}_aP_b$ consists of a rational function of δ which is a polynomial of ath order divided by a polynomial of bth order. If the series in Equation 14 is known to cth order, then one can construct a Padé representation of order $(a + b) = c$. Note that the ${}_1P_1$ Padé only uses coefficients up to second order in δ, while the ${}_1P_2$ and ${}_2P_1$ use coefficients up to third order in δ. The Padé values are closer to the exact value of the ground state energy than the values shown in Table 2.

It is not clear from the data presented, however, exactly what criteria determine when Padé summation is needed. A more complete study of how different values of λ and δ effect the approximate energy eigenvalues might reveal the answer to this question.

ACKNOWLEDGMENTS

The author would like to thank Dr. Lawrence R. Mead for his support and guidance in producing this paper. He would also like to thank the USM-NASA Space Grant College and Fellowship Program, under Grant No. NASA NGT-40028, for making this work possible.

	Order by order results	
Order	$\delta = 3$; $\lambda = 0.1$	$\delta = 3$; $\lambda = 1.0$
Zeroth	0.54772	0.86603
First	0.53938	0.60962
Second	0.69981	1.44677
Third	0.47885	-0.34878
Exact	0.62051	0.82069

Table 2

The ground state delta expansion energy values for zeroth, first, second and third order perturbation for the anharmonic octic potential. As more terms are considered, the δ-expansion approximation strays further from the exact values.

Padé Summation for Ground State Energy				
	$\lambda = 0.1$	% error	$\lambda = 1.0$	% error
${}_1P_1$	.54743	12	.80591	2.4
${}_1P_2$	.61670	.61	.88830	8.2
${}_2P_1$	.60832	2.1	.87582	6.7

Table 3

The Padé summation of the δ-expansion for the ground state energy of the anharmonic octic oscillator. The table also shows the percent error in the energies. The exact energies were determined by matrix diagonalization taken from reference 6.

REFERENCES

* Current address of the author: Department of Physics, University of Arizona, Tucson, AZ 85719 gittings@soliton.physics.arizona.edu

1. D.J. Griffiths, Introduction to Quantum Mechanics, (Addison-Wesley), 1995.
2. J.L Powell and B. Crasemann, Quantum Mechanics, (Addison-Wesley), 1961.
3. C.M. Bender and T.T. Wu, Phys. Rev., 184, (1969), p. 1231; C.M. Bender and T.T. Wu, Phys. Rev. D., 7, (1973), p. 1620.
4. C.M Bender, H.A. Milton, S. Pinsky and L.M. Simmons, Jr., J. Math. Phys., 30, (1989), p. 1447.
5. C-S. Hsue and J.L. Chern, Phys. Rev. D., 29, (1984), p. 643.
6. F.T. Hioe, D. MacMillen and E.W. Montroll, J. Math. Phys., 17, (1976), p. 1320.
7. C.M. Bender and S.A. Orzag, Advanced Mathematical Methods for Scientists and Engineers, (McGraw-Hill), 1978, Ch. 8.

FACULTY SPONSOR

Dr. Lawrence R. Mead
Department of Physics and Astronomy
University of Southern Mississippi
Hattiesburg, MS 39406-5046
lrmead@whale.st.usm.edu

PREPARING A MANUSCRIPT FOR PUBLICATION

Rexford E. Adelberger, Editor

Perhaps the most important thing for you to keep in mind when you write a manuscript which you intend to submit for publication to the Journal of Undergraduate Research in Physics is that the audience that will be reading the paper is junior or senior physics majors. They are knowledgeable about physics, but unlike you, they have not spent as much time trying to understand the specific work which is being reported in your paper. They also can read English well, and expect the paper to be written by a colleague, not a robot or an 'all-knowing' computer. There is a big difference between the comments you write in the margin of your lab notebook or what you might write in a technical brief and what you should present in a paper for publication in a scientific journal.

There is a significant difference between a Journal article and keeping a journal. Your laboratory data book should be the journal of what you did. It contains all the data, what you did (even if it was an attempt that turned out to be wrong), as well as comments as to what you were thinking at that time. The Journal article is an discussion of how you would do the research without excursions along blind alleys and hours spent collecting data that were not consistent. The reader should not necessarily be able to completely reproduce the work from the Journal article, but the reader should be able to understand the physics and techniques of what was done.

How a person uses Journal articles to find out about new ideas in physics is often done in the following way. A computerized search, using key words in abstracts, is performed to find what work others have done in the area of interest. If the abstract seems to be about the question of interest, the body of the paper is tracked down and read. If the reader then wants to find out the finer details of how to reproduce the experiment or the derivation of some equation, the author of the paper is contacted for a personal in-depth conversation about the more subtle details.

The general style of writing that should be followed when preparing a manuscript for publication in the Journal is different from what you would submit to your English literature professor as a critique of some other work. The narrative of the paper is intended to do three things: 1) present the background necessary for the reader to appreciate and understand the physics being reported in the paper; 2) discuss the details of what you did and the implications of your work; 3) lead the reader through the work in such a way that they must come to the same concluding points that you did. When finished with your paper, the reader should not have to go back and try to decide for themselves what you did. Your narrative should lead them through your work in an unambiguous manner, telling them what to see and understand in what you did. The interpretation of the data or calculations should be done by the writer, not the reader. The interpretation of your results is the most important part of the paper.

You should take care to make sure that the material is presented in a concise logical way. You should make sure that your sentences do not have too many dependent clauses. Overly complicated sentences make the logic of an argument difficult to follow. You should choose a paragraph structure that focuses the attention of the reader on the development of the ideas.

A format which often achieves these aims is suggested below:

ABSTRACT : An abstract is a self contained paragraph that concisely explains what you did and presents any interesting results you found. The abstract is often published separately from the body of the paper, so you cannot assume that the reader of the abstract also has a copy of the rest of the paper. You cannot refer to figures or data that are presented in the body of the paper. Abstracts are used in computerized literature searches, so all key words that describe the paper should be included in the abstract.

INTRODUCTION: This is the section that sets the background for the important part of the paper. It is not just an abbreviated review of what you are going to discuss in detail later. This section of the narrative should present the necessary theoretical and experimental background such that a knowledgeable colleague, who might not be expert in the field, will be able to understand the data presentation and discussion. If you are going to use a particular theoretical model to extract some formation from your data, this model should be discussed in the introduction.

Where appropriate, factual information should be referenced using end-notes. When presenting background information, you can guide the reader to a detailed description of a particular item with the statement such as: *"A more detailed discussion of laminar flow can be found elsewhere [1]"*. If you know where there is a good discussion of some item, you don't have to repeat it, just guide the reader to the piece.

How one proceeds from this point depends upon whether the paper is about a theoretical study or is a report on an experiment. I will first suggest a format for papers about experimental investigations and then one that describes a theoretical derivation.

Experimental Investigations

THE EXPERIMENT: This section guides the reader through the techniques and apparatus used to generate the data. Schematic diagrams of equipment and circuits are often easier to understand than prose descriptions. A statement such as *"A diagram of the circuit used to measure the stopping potential is shown in Figure 6"* is better than a long elegant set of words. It is not necessary to describe in words what is shown in a diagram unless you feel that there is a very special part which should be pointed out to the reader. If special experimental techniques were developed as part of this work, they should be discussed here. You should separate the discussion of the equipment used to measure something from your results. This section should not include data presentations or discussions of error analysis.

DATA PRESENTATION AND INTERPRETATION OF RESULTS: This is the most important section of the paper. The data *(a plural noun)* are the truths of your work. This section should lead the reader through the data and how errors were measured or assigned. The numerical data values are presented in tables and figures, each with its own number and caption, e.g.. *"The results of the conductivity measurements are shown in Table 3"*. It is difficult to follow narratives where the numerical results are included as part of the narrative. Raw, unanalyzed data should not be presented in the paper. All figures and tables should be referred to by their number. Any figure or table that is not discussed in the narrative should be eliminated. Items which are not discussed have no place in a paper.

A Theoretical Study

THE MODEL: This part should consist of a theoretical development of the constructs used to model the physical system

under investigation. Formulae should be on separate lines and numbered consecutively. The letters or symbols used in the equations should be identified in the narrative, e.g.. *The potential can be approximated as:*

$$W \approx Z - \sigma(\rho) \ , \qquad (1)$$

where Z is the number of protons and σ is the screening constant that is dependent on the charge density, ρ, of the inner electrons of the K and L shells. If you wish to use this formula at a later time in the narrative, you refer to it by its number, e.g.. *"The straight line fit shown in Figure 3 means that we can use Equation 1 to extract a value of..."*

CALCULATIONS: This section presents a summary and discussion of the numerical results calculated from the model. The results should be presented in tables or graphs, each with a caption. A table or graph which is not discussed in the narrative should be eliminated. Data that are not interpreted by the writer have no place in a paper. One should reference numerical results that are used in the calculations and come from previous work done by others .

The following sections pertain to both types of papers.

CONCLUSIONS: It is indeed rare that one can come to clear and meaningful conclusions in one paper. I do not know of many papers where this section should be included.

REFERENCES: All references, numbered in order from beginning to end of the paper, are collected together at the end of the paper. You should be aware of the following format:

If the reference is a text-

1. A.J. Smith and Q.C.S. Smythe, Electromagnetic Theory, Addison Wesley, New York, (1962), p. 168.

If the reference is a journal-

2. J. Boswain, Journal of Results, 92, (1968), pp. 122-127.

If the reference is unpublished-

3) R.J. Ralson, private communication.

ACKNOWLEDGMENTS: This short section should acknowledge the help received (that is not referenced in the previous section) from others. This is where you would give credit to a lab partner or someone in the machine shop who helped you build a piece of equipment.

OTHER ADVICE

TABLES AND FIGURES are placed by the layout editors at the corners of the page to make the format attractive and easy to read. Often a figure is not on the same page as the discussion of the figure. Each table or figure should be numbered and have a caption which explains the figure. Readers scan papers by looking at the figures and data tables before they read the narrative of the work. Take care to put enough information in the caption of a figure or table so that the reader can get some feeling for the meaning of the data presentation. All lines shown on graphs should be identified, e.g.. *"The dashed line is drawn to guide the eye"* or *"The solid line is a fit to the data using the Ising model"*

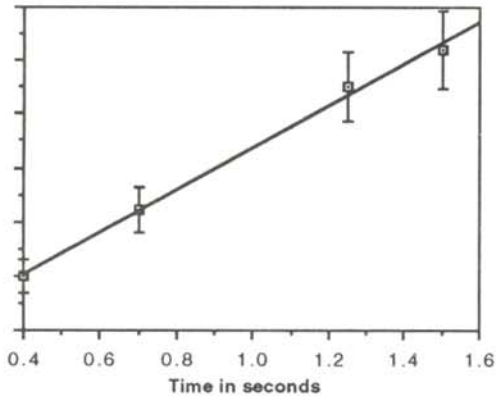

Figure 1

A graph of the measured thrust of a D-2 model rocket engine as a function of time. The line drawn is the least squares fit straight line to the data.

State	*Experimental eV*	*Theoretical eV*
3S	*5.15±01*	*5.13*
4S	*1.89±02*	*1.93*
3P	*2.96±02*	*3.02*

Table 1

Energy states found in the numerical search. The accepted values for these states are also listed.

An example of a graph of a set of data is shown in Figure 1. The graph is sized by the range of data points. The bottom left point does not have to be the point (0,0). Error bars are shown with the data points. A graph with all the data points clustered in one small corner and lots of white space does not help the reader get a feeling of the dependence of your data. Be careful that the figures you present are not too busy; too much information on a figure makes it difficult to pick out the important parts.

NUMBERS AND UNITS Any experimentally measured data presented in tables (such as shown in Table 1), should include an uncertainty. You should use scientific notation when presenting numbers, $(7.34 \pm .03) \times 10^7$ eV. Take care that you have the correct number of significant digits in your results; just because the computer prints out 6 digits does not mean that they are significant. You should use the MKS system of units.

STYLE It is often helpful to make a flow chart of your paper before you write it. In this way, you can be sure that the logical development of your presentation does not resemble two octopuses fighting, but that it is linear.

One generally writes the report in the past tense. You already did the experiment. You also should use the third person neuter case. Even though you might have done the work by yourself, you use "we". e.g.. *"We calculated the transition probability for..."* It is often confusing when you begin sentences with conjunctions. Make sure that each sentence is a clear positive statement rather than an apology.

There are a few words or phrases you should be careful about using. ***Fact*** - this is a legal word. I am not sure what it means in physics. ***Proof or prove*** - These words are meaningful in mathematics, but you can't prove something in physics, especially experimental physics. ***The purpose of this experiment is...*** Often it is necessary to do the experiment to complete the requirements for your degree. You do not need to discuss the purposes of the experiment. ***One can easily show that...*** - Don't try to intimidate the reader. What if the reader finds it difficult to show? Remember that the reader of your paper is a senior in college! ***It is obvious that... or One clearly can see....*** - Such statements only intimidate the reader that does not find your work trivial. What is obvious to someone who has spent a lot of time thinking about it may not be obvious to the reader of your paper.

The Journal of Undergraduate Research in Physics

The Journal of Undergraduate Research in Physics is the journal of Sigma Pi Sigma and the Society of Physics Students. It is published by the Physics Department of Guilford College, Greensboro NC 27410. Inquiries about the journal should be sent to the editorial office.

The Journal of Undergraduate Research in Physics ISSN 0731-3764

Editorial Office -

The Journal of Undergraduate Research in Physics
Physics Department
Guilford College
Greensboro, NC 27410
336-316-2279 (voice)
336-316-2951 (FAX)

Editor -

Dr. Rexford E. Adelberger
Professor of Physics
Physics Department
Guilford College
Greensboro, NC 27410
ADELBERGERRE@RASCAL.GUILFORD.EDU

The Society of Physics Students

National Office -

Dr. Dwight Neuenschwander, Director
Ms. Sonja Lopez, SPS Supervisor
Society of Physics Students
American Institute of Physics
1 Physics Ellipse
College Park, MD 20740
301-209-3007

President of the Society -

Dr. Robert Fenstermacher
Department of Physics
Drew University

President of Sigma Pi Sigma -

Dr. Jean Krisch
Department of Physics
University of Michigan, Ann Arbor